

1 **Coulomb stress interactions among  $M \geq 5.9$  earthquakes**  
 2 **in the Gorda deformation zone and on the Mendocino Fault Zone,**  
 3 **Cascadia subduction zone, and northern San Andreas Fault**

4 John C. Rollins<sup>1</sup> and Ross S. Stein<sup>2</sup>

5 Received 8 November 2009; revised 14 June 2010; accepted 8 July 2010; published XX Month 2010.

6 [1] The Gorda deformation zone, a 50,000 km<sup>2</sup> area of diffuse shear and rotation offshore  
 7 northernmost California, has been the site of 20  $M \geq 5.9$  earthquakes on four different fault  
 8 orientations since 1976, including four  $M \geq 7$  shocks. This is the highest rate of large  
 9 earthquakes in the contiguous United States. We calculate that the source faults of six  
 10 recent  $M \geq 5.9$  earthquakes had experienced  $\geq 0.6$  bar Coulomb stress increases imparted  
 11 by earthquakes that struck less than 9 months beforehand. Control tests indicate that  
 12  $\geq 0.6$  bar Coulomb stress interactions between  $M \geq 5.9$  earthquakes separated by  $< 9$  months  
 13 are unlikely to occur by random chance, suggesting that the multiple short-term stress  
 14 interactions observed among the recent Gorda zone earthquakes are not an apparent effect.  
 15 In all well-constrained  $\geq 0.2$  bar Coulomb stress interactions between earthquakes that  
 16 occurred within 4 years of each other, the second earthquake is promoted. On longer  
 17 timescales, calculated stress changes imparted by the 1980  $M_w = 7.3$  Trinidad earthquake  
 18 are consistent with the locations of  $M \geq 5.9$  earthquakes in the Gorda zone until at least  
 19 1995, as well as earthquakes on the Mendocino Fault Zone in 1994 and 2000. Coulomb  
 20 stress changes imparted by the 1980 earthquake are also consistent with its distinct  
 21 elbow-shaped aftershock pattern. From these observations, we derive generalized static  
 22 stress interactions among right-lateral, left-lateral and thrust faults near triple junctions.

23 **Citation:** Rollins, J. C., and R. S. Stein (2010), Coulomb stress interactions among  $M \geq 5.9$  earthquakes in the Gorda  
 24 deformation zone and on the Mendocino Fault Zone, Cascadia subduction zone, and northern San Andreas Fault, *J. Geophys.*  
 25 *Res.*, 115, XXXXXX, doi:10.1029/2009JB007117.

26 **1. Introduction**

27 [2] The Gorda deformation zone is the southernmost  
 28 section of the Juan de Fuca plate, bounded by the Gorda  
 29 Ridge on the west, the Cascadia subduction zone on the east,  
 30 and the Mendocino Fault Zone on the south (Figure 1). At  
 31 the southeast corner of the Gorda zone, the North American,  
 32 Pacific and Juan de Fuca plates meet at the Mendocino  
 33 Triple Junction. The Juan de Fuca plate generally moves  
 34 20°–30° south of east relative to the Pacific plate, but the  
 35 Mendocino Fault Zone strikes east-west, causing a space  
 36 problem within the Gorda deformation zone that results in  
 37 north-south compression and east-west extension. The  
 38 space problem also slows spreading rates at the Gorda Ridge  
 39 from 52 mm/yr at 42°N to 25 mm/yr at 40.5°N (Wilson  
 40 [1989], with Cande and Kent's [1995] timescale correc-  
 41 tion), which causes the Gorda zone to rotate clockwise. The  
 42 compression, extension and rotation are accommodated by

internal deformation along northeast striking left-lateral 43  
 faults [Wilson, 1986; Chaytor et al., 2004]. Since 1976,  $M \geq$  44  
 5.9 earthquakes have ruptured several of those left-lateral 45  
 faults as well as the right-lateral Mendocino Fault Zone, the 46  
 southernmost Cascadia subduction zone, and northwest 47  
 striking right-lateral faults near Cape Mendocino. In addi- 48  
 tion, the rupture zone of the 1700  $M \sim 9$  Cascadia earth- 49  
 quake may have extended into this region, and the 1906 San 50  
 Francisco earthquake ruptured the San Andreas Fault to the 51  
 Mendocino Triple Junction. 52

2. Sources for Faults 53

[3] We use the Chaytor et al. [2004] surface traces of the 54  
 Mendocino Fault Zone and faults in the Gorda deformation 55  
 zone; those faults are assumed to be vertical. We use the 56  
 McCrory et al. [2004] surface traces of the Gorda Ridge and 57  
 Cascadia subduction zone. The Cascadia subduction zone 58  
 dips 9° under northern California [Jachens and Griscom, 59  
 1983]; we assume that it strikes 350° in this region (from 60  
 the surface trace and the Oppenheimer et al. [1993] model 61  
 of the 1992 Cape Mendocino shock) and has a rake of 62  
 90°. The northernmost San Andreas and local faults near 63  
 Cape Mendocino are from the USGS Quaternary Fault and 64

<sup>1</sup>Department of Earth Sciences, University of Southern California, Los Angeles, California, USA.

<sup>2</sup>U.S. Geological Survey, Menlo Park, California, USA.

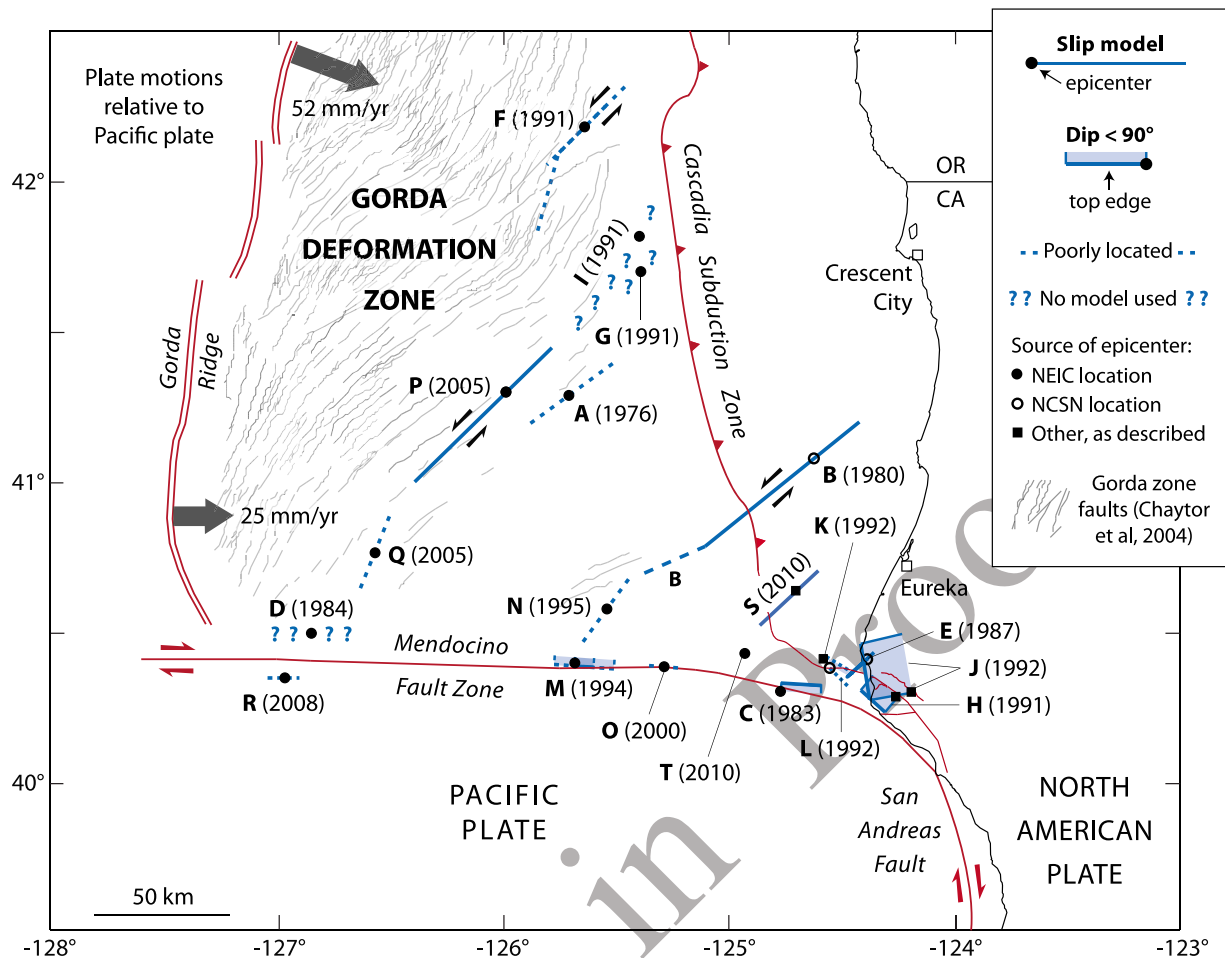


**Figure 1.** Tectonic configuration of the Gorda deformation zone and locations and source models for 1976–2010  $M \geq 5.9$  earthquakes. Letters designate chronological order of earthquakes (Table 1 and Appendix A). Plate motion vectors relative to the Pacific Plate (gray arrows in main diagram) are from Wilson [1989], with Cande and Kent's [1995] timescale correction.

65 Fold Database (<http://earthquake.usgs.gov/hazards/qfaults>)  
66 and McPherson and Dengler [1992].

### 67 3. Source Parameters for 1976–2010 Earthquakes

68 [4] Because all local seismic stations lie to the east of the  
69 offshore Gorda deformation zone, earthquake locations are  
70 prone to error, particularly in the east-west direction. We  
71 handle these uncertainties on a case-by-case basis for the  
72 recent  $M \geq 5.9$  earthquakes. The Northern California Seis-  
73 mic Network (NCSN) catalog and the northern California  
74 double-difference catalog [Waldhauser and Schaff, 2008]  
75 generally provide the most accurate locations for earth-  
76 quakes close to the coast, but their coverage extends only to  
77 100–150 km offshore; the double-difference catalog is more  
78 accurate than NCSN but does not cover the period 1976–  
79 1983 (Table 1). The USGS National Earthquake Information  
80 Center (NEIC) catalog provides the best locations for  
81 earthquakes further offshore, as locations from the under-  
82 water SOSUS network appear to have significant westerly  
83 biases and magnitude errors in our study area. We obtain  
84 aftershock locations for the 1980  $M_w = 7.3$  earthquake from  
85 the Hill *et al.* [1990] plot of 1980–1986 northern California

seismicity (with relocations by J.P. Eaton), as these loca- 86  
tions were not incorporated into the NCSN catalog. Unless 87  
otherwise indicated, we obtain strike, dip, rake, and scalar 88  
moment values for  $M \geq 5.9$  earthquakes from the Global 89  
CMT catalog. (It should be noted that NCSN and NEIC 90  
local magnitudes for two earthquakes in 1983 and 1987 are 91  
less than 5.9, but the Global CMT moment magnitudes are 92  
6.1 and 6.0, respectively, so both shocks are included.) 93

### 4. Slip Models for 1976–2010 $M \geq 5.9$ Earthquakes

[5] Slip models exist in the literature for the 1992  $M_w =$  96  
6.9 Cape Mendocino, 2005  $M_w = 7.2$ , and 2010  $M = 6.5$  97  
earthquakes (Figure 2, Table 1, and Appendix A). For most 98  
of the other  $M \geq 5.9$  shocks, we construct simple source 99  
models using main shock source parameters. For  $M < 6.5$  100  
earthquakes, the source length and width are determined by 101  
empirical scaling relations from Wells and Coppersmith 102  
[1994]. We assume that the seismogenic thickness of the 103  
Gorda zone is 9–10 km [Smith *et al.*, 1993; Henstock and 104  
Levander, 2003], which constrains the downdip width of 105  
 $M \geq 6.5$  earthquakes on vertical faults, so for  $M \geq 6.5$  106

Table 1. Source Parameters Used for 1976–2010  $M \geq 5.9$  Earthquakes

| ID    | General Parameters       |            |       |               |                | Focal Mechanism |                               |           |         |           | Rupture Model Parameters |                                      |                  |              |                    |                    |  |
|-------|--------------------------|------------|-------|---------------|----------------|-----------------|-------------------------------|-----------|---------|-----------|--------------------------|--------------------------------------|------------------|--------------|--------------------|--------------------|--|
|       | Date <sup>a</sup>        | Time (UTC) | $M_w$ | Latitude (°N) | Longitude (°W) | Depth (km)      | Reference                     | Strike    | Dip     | Rake      | Moment (dyn cm)          | Reference                            | Length (km)      | Width (km)   | Average Slip (m)   | Stress Drop (bars) |  |
| t1.4  | A 11/26/1976             | 1119       | 6.7   | 41.29         | 125.71         | 15              | NEIC catalog                  | 54°       | 85°     | 5°        | $1.36 \times 10^{26}$    | Global CMT NP1                       | 40.0             | 10.0         | 1.1                | 16                 |  |
| t1.5  | B 11/8/1980              | 1027       | 7.3   | 41.085        | 124.618        | 14.2            | NCSN catalog                  | 51°       | 89°     | 27°       | $1.12 \times 10^{27}$    | Global CMT NP2                       | 100.0            | 10.0         | 3.6                | 68                 |  |
| t1.6  | C 8/24/1983              | 1336       | 6.1   | 40.31         | 124.77         | 30              | NEIC catalog                  | 93°       | 65°     | 153°      | $2.09 \times 10^{25}$    | Global CMT NP1                       | 15.4             | 7.7          | 0.6                | 15                 |  |
| t1.7  | D 9/10/1984              | 0314       | 6.6   | 40.50         | 126.83         | 10              | NEIC catalog                  | 270°      | 66°     | 178°      | $1 \times 10^{26}$       | Global CMT NP1                       | -                | -            | -                  | -                  |  |
| t1.8  | E 7/31/1987              | 2356       | 6.0   | 40.416        | 124.383        | 17.6            | NCSN catalog                  | 226°      | 90°     | 0°        | $1.19 \times 10^{25}$    | Global CMT NP2                       | 13.2             | 7.1          | 0.4                | 11                 |  |
| t1.9  | F <sup>b</sup> 7/13/1991 | 0250       | 6.8   | 42.182        | 125.641        | 11              | NEIC catalog                  | 225°      | 88°     | -12°      | $2.06 \times 10^{26}$    | Global CMT NP2                       | 40 (1)<br>55 (2) | 10.0<br>10.0 | 1.4 (1)<br>1.1 (2) | 27 (1)<br>20 (2)   |  |
| t1.10 | G 8/16/1991              | 2226       | 6.3   | 41.697        | 125.385        | 10              | NEIC catalog                  | 40°       | 68°     | 6°        | $3.13 \times 10^{25}$    | Global CMT NP1                       | -                | -            | -                  | -                  |  |
| t1.11 | H 8/17/1991              | 1929       | 6.1   | 40.286        | 124.246        | 9.3             | Walthausser and Schaff [2008] | 311°      | 22°     | 51°       | $1.9 \times 10^{25}$     | Global CMT NP1                       | 12.0             | 7.7          | 0.6                | 22                 |  |
| t1.12 | I 8/17/1991              | 2217       | 7.1   | 41.821        | 125.397        | 13              | NEIC catalog                  | 46°       | 86°     | 28°       | $4.43 \times 10^{26}$    | Global CMT NP2                       | -                | -            | -                  | -                  |  |
| t1.13 | J 4/25/1992              | 1806       | 6.9   | 40.301        | 124.197        | 9.6             | Oppenheimer et al. [1993]     | 350°      | 12°     | 94°       | $2.79 \times 10^{26}$    | Oppenheimer et al. [1993]            | 21.0             | 16.0         | 3.3                | 49                 |  |
| t1.14 | K 4/26/1992              | 0741       | 6.5   | 40.415        | 124.603        | 20.4            | Walthausser and Schaff [2008] | 122.3°    | 75.9°   | 175.2°    | $6.35 \times 10^{25}$    | Oppenheimer et al. [1993]            | 12.0             | 6.4          | 2.6                | 78                 |  |
| t1.15 | L 4/26/1992              | 1118       | 6.6   | 40.383        | 124.555        | 22.6            | NCSN catalog                  | 311.2°    | 89.6°   | 181.8°    | $1.20 \times 10^{26}$    | Oppenheimer et al. [1993]            | 10.0             | 5.0          | 7.6                | 290                |  |
| t1.16 | M 9/1/1994               | 1515       | 7.0   | 40.40         | 125.68         | 10              | NEIC catalog                  | 274°      | 65°     | 176°      | $3.88 \times 10^{26}$    | Global CMT NP1                       | 15.0             | 7.5          | 10.9               | 280                |  |
| t1.17 | N 2/19/1995              | 0403       | 6.6   | 40.56         | 125.54         | 10              | NEIC catalog                  | 216°      | 87°     | -18°      | $9.95 \times 10^{25}$    | Global CMT NP2                       | 30.0             | 10.0         | 1.0                | 19                 |  |
| t1.18 | O 3/16/2000              | 1519       | 5.9   | 40.39         | 125.28         | 7               | NEIC catalog                  | 275°      | 88°     | 180°      | $7.75 \times 10^{24}$    | Global CMT NP1                       | 11.3             | 6.5          | 0.3                | 10                 |  |
| t1.19 | P 6/15/2005              | 0250       | 7.2   | 41.29         | 125.95         | 16              | NEIC catalog                  | 47°       | 85°     | -3°       | $8.3 \times 10^{26}$     | Shao and Ji (2005)                   | 72.0             | 20.0         | 1.4                | 21                 |  |
| t1.20 | Q 6/17/2005              | 0621       | 6.6   | 40.77         | 126.57         | 12              | NEIC catalog                  | 202°      | 89°     | -8°       | $1.14 \times 10^{26}$    | Global CMT NP2                       | 30.0             | 10.0         | 1.2                | 23                 |  |
| t1.21 | R 11/28/2008             | 1342       | 5.9   | 40.35         | 126.98         | 10              | NEIC catalog                  | 270°      | 85°     | 176°      | $1.03 \times 10^{25}$    | Global CMT NP1                       | 11.8             | 6.5          | 0.4                | 12                 |  |
| t1.22 | S 1/10/2010              | 0027       | 6.5   | 40.652        | 124.692        | 29.3            | USGS/NEIC                     | 227°      | 81°     | 6°        | $8.0 \times 10^{25}$     | D. Dreger (unpublished report, 2010) | 30.0             | 20 (max)     | 0.78               | ~12                |  |
| t1.23 | T 2/4/2010               | 2020       | 5.9   | 40.412        | 124.961        | 23.6            | USGS/NEIC                     | 215°/306° | 79°/85° | -5°/-169° | $9.19 \times 10^{24}$    | Global CMT                           | -                | -            | -                  | -                  |  |
| t1.24 |                          |            |       |               |                |                 |                               |           |         |           |                          |                                      |                  |              |                    |                    |  |
| t1.25 |                          |            |       |               |                |                 |                               |           |         |           |                          |                                      |                  |              |                    |                    |  |

<sup>a</sup>Dates are given as month/day/year.<sup>b</sup>Values for both models 1 and 2 (as indicated in parentheses) are given for length, average slip, and stress drop.

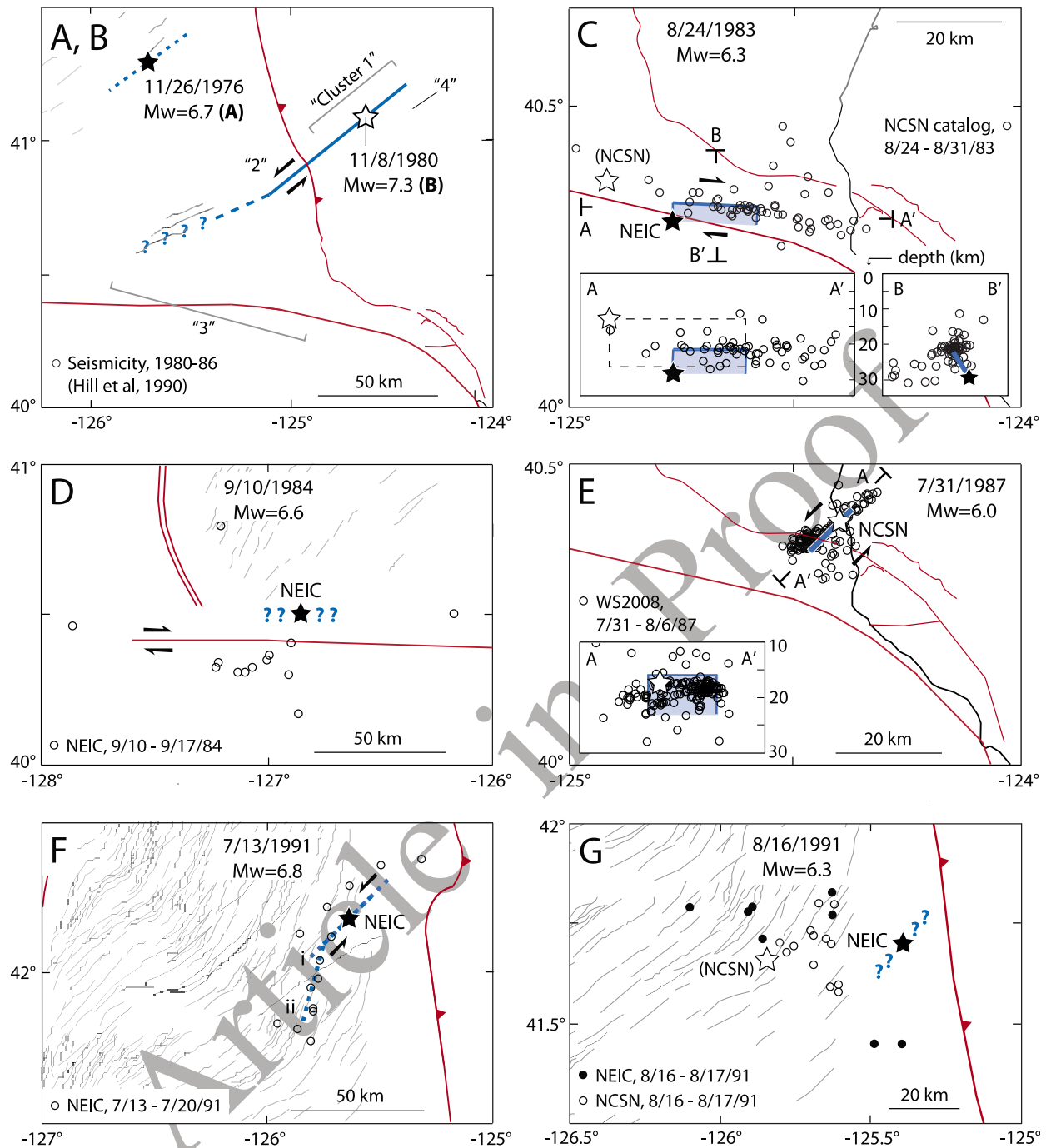


**Figure 2.** Source models for earthquakes A and B, 26 November 1976,  $M_w = 6.7$ , and 8 November 1980,  $M_w = 7.3$ ; C, 24 August 1983,  $M_w = 6.1$  (poorly constrained); D, 10 September 1984,  $M_w = 6.6$  (no model made); E, 31 July 1987,  $M_w = 6.0$ , “WS2008” refers to Waldhauser and Schaff’s [2008] double-difference catalog; F, 13 July 1991,  $M_w = 6.8$  (poorly constrained); G, 16 August 1991 (2226 UTC),  $M_w = 6.3$  (no model made), open circles are NCSN locations for 16 August 1991 (2226 UTC) to 17 August 1991 (2216 UTC); H, 17 August 1991 (1929 UTC),  $M_w = 6.1$ ; I, 17 August 1991 (2217 UTC),  $M_w = 7.1$  (no model made); J, 25 April 1992,  $M_w = 6.9$ , open circles are from Waldhauser and Schaff’s [2008] earthquake locations for 25 April 1992 (1806 UTC) to 26 April 1992 (0741 UTC); K and L, 26 April 1992 (0741 UTC),  $M_w = 6.5$  and 26 April 1992 (1118 UTC),  $M_w = 6.6$  (both poorly constrained), seismicity shallower than 15 km was excluded so that shallow aftershocks of (J) do not crowd figure; M, 1 September 1994,  $M_w = 7.0$ ; N and O, 19 February 1995,  $M_w = 6.6$ , and 16 March 2000,  $M_w = 5.9$ ; P, Q, and R, 15 June 2005,  $M_w = 7.2$ , 17 June 2005,  $M_w = 6.6$  (poorly constrained), and 28 November 2008,  $M_w = 5.9$  (poorly constrained); S and T, 10 January 2010,  $M = 6.5$ , and 4 February 2010,  $M_w = 5.9$ ; Z, 18 April 1906,  $M = 7.8$ .

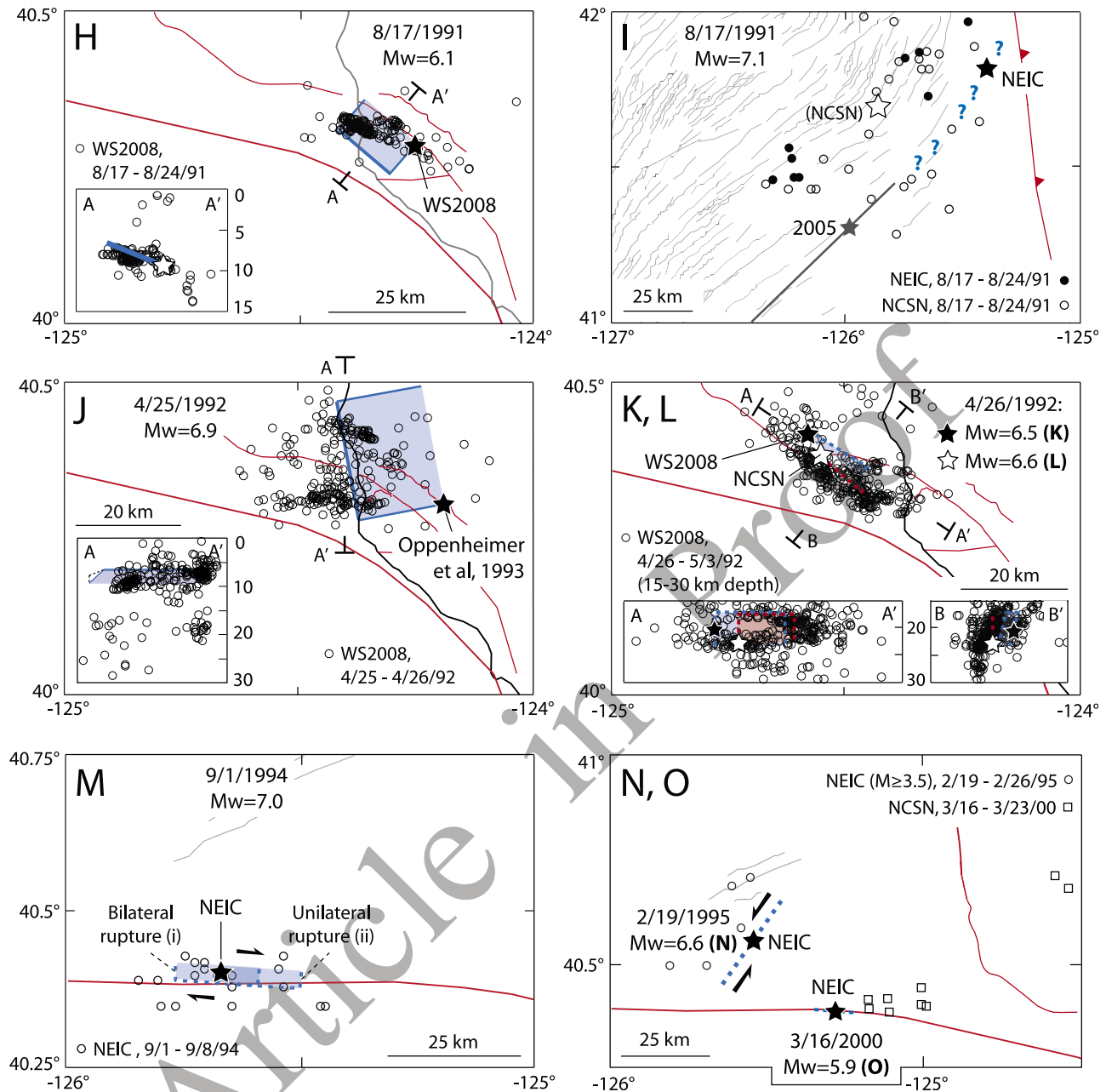


Figure 2. (continued)

107 earthquakes we assume a width of 10 km and set the source  
 108 length equal to that of the aftershock pattern. The stress drop  
 109 is kept between 10 and 100 bars, with the exception of two  
 110 earthquakes in 1992 and 1994 for which *Choy and McGarr*  
 111 [2002] observed high apparent stress values. We assume a  
 112 bilateral rupture if the main shock hypocenter is in the  
 113 middle of the aftershock pattern and a unilateral rupture if  
 114 the hypocenter is at one end. If aftershocks are consistent  
 115 with the best main shock location but do not indicate a fault  
 116 plane, we conclude that the source model is poorly located,  
 117 and so stress interactions calculated with it are tentative. If  
 118 aftershocks are inconsistent with the best main shock loca-  
 119 tion, we do not make a source model for the main shock. All

source models are shown in Figure 2 and described in the  
 Appendix A. The letters used to refer to the earthquakes  
 throughout the rest of the text are keyed to Tables 1 and 2,  
 Figures 1 and 2, and Appendix A.

## 5. Calculation of Static Stress Transfer

[6] The rupture of a fault in an earthquake deforms the  
 surrounding crust, changing the static stress on nearby faults  
 depending on their orientations. The Coulomb stress change  
 is defined as  $\Delta CFF = \Delta\tau + \mu\Delta\sigma$ , where  $\tau$  is the shear stress  
 on the fault (positive in the inferred direction of slip),  $\sigma$  is

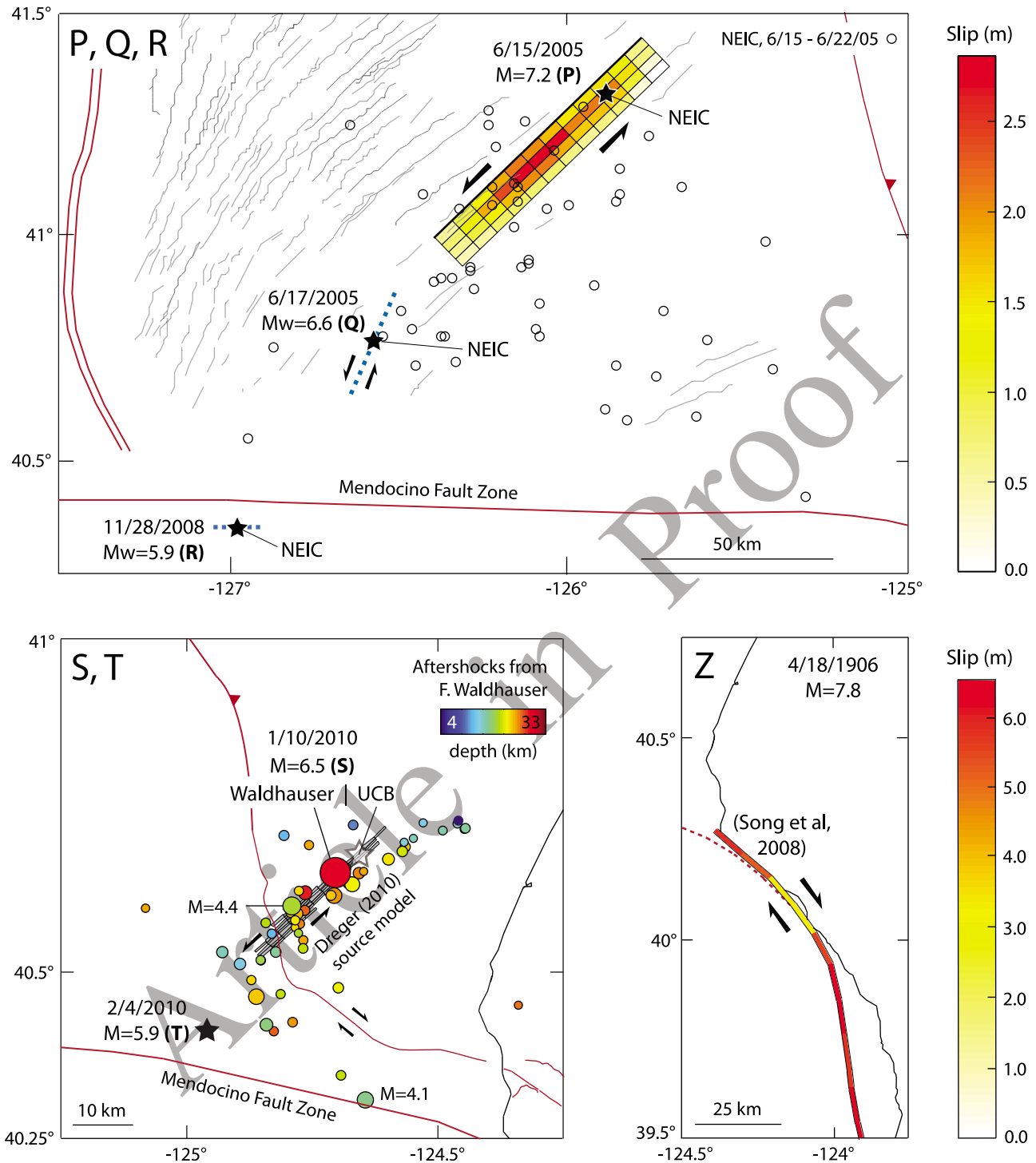


Figure 2. (continued)

130 the normal stress (positive for unclamping), and  $\mu$  is the  
 131 apparent friction coefficient [King *et al.*, 1994].  
 132 [7] We perform two kinds of calculations using Cou-  
 133 lomb 3.1 (<http://earthquake.usgs.gov/research/modeling/>).  
 134 The first determines the Coulomb stress change imparted by  
 135 a source earthquake to the epicenter of a subsequent receiver  
 136 earthquake given its orientation and rake. The rupture of the

137 receiver earthquake is promoted if the imparted stress  
 138 change is positive and inhibited if the stress change is  
 139 negative. We run this calculation for all source models. The  
 140 second method determines the stress changes imparted by a  
 141 source earthquake to surrounding faults; these can be com-  
 142 pared with aftershocks and changes in seismicity rates. We  
 143 run this calculation for the 1980  $M_w = 7.3$ , 1992  $M_w = 6.9$ , 143

**Table 2.** Coulomb Stress Interactions  $\geq 0.5$  bar Among 1976–2010  $M \geq 5.9$  Earthquakes

| ID | Source Earthquake |       |  | Receiver Earthquake |                   |       | Time Between Earthquakes (years) | Imparted Coulomb Stress Change (bars)  |
|----|-------------------|-------|--|---------------------|-------------------|-------|----------------------------------|--|
|    | Date <sup>a</sup> | $M_w$ |  | ID                  | Date <sup>a</sup> | $M_w$ |                                  |  |
| A  | 11/26/1976        | 6.7   |  | I                   | 8/17/1991         | 7.1   | 14.7                             | Poorly constrained   |
| B  | 11/8/1980         | 7.3   |  | P                   | 6/15/2005         | 7.2   | 28.5                             | Likely negative but poorly constrained   |
| C  | 8/24/1983         | 6.1   |  | M                   | 9/1/1994          | 7.0   | 13.8                             | +0.7 or more <sup>b</sup>  |
| D  | 9/10/1984         | 6.6   |  | N                   | 2/19/1995         | 6.6   | 14.3                             | Large but poorly constrained <sup>b</sup>  |
| E  | 7/31/1987         | 6.0   |  | O                   | 3/16/2000         | 5.9   | 19.4                             | +2   |
| F  | 8/16/1991         | 6.3   |  | P                   | 6/15/2005         | 7.2   | 24.7                             | -0.5   |
| G  | 8/16/1991         | 6.3   |  | K                   | 4/26/1992         | 6.5   | 8.7                              | +0.5 (poorly constrained)  |
| H  | 8/17/1991         | 6.1   |  | R                   | 11/28/2008        | 5.9   | 24.2                             | Large but poorly constrained   |
| I  | 8/17/1991         | 7.1   |  | L                   | 4/26/1992         | 6.6   | 4.7                              | -2   |
| J  | 4/25/1992         | 6.9   |  | I                   | 8/17/1991         | 7.1   | 0.003                            | Large but poorly constrained   |
| K  | 4/26/1992         | 6.5   |  | J                   | 4/25/1992         | 6.9   | 0.69                             | +1 (at 1992 epicenter) to +4   |
| L  | 4/26/1992         | 6.6   |  | P                   | 6/15/2005         | 7.2   | 13.8                             | Large but poorly constrained   |
| M  | 9/1/1994          | 7.0   |  | K                   | 4/26/1992         | 6.5   | 0.0016                           | +0.9   |
| N  | 2/19/1995         | 6.6   |  | L                   | 4/26/1992         | 6.6   | 0.0019                           | +3   |
| O  | 3/16/2000         | 5.9   |  | L                   | 4/26/1992         | 6.6   | 0.0003                           | Large but poorly constrained   |
| P  | 6/15/2005         | 7.2   |  | T                   | 2/4/2010          | 5.9   | 17.8                             | -0.6 on SW striking nodal plane/-0.3 on NW striking nodal plane (poorly constrained) |
| Q  | 6/17/2005         | 6.6   |  |                     |                   |       |                                  | +3 to +10  |
| R  | 11/28/2008        | 5.9   |  |                     |                   |       |                                  | +2 to +6   |
| S  | 1/10/2010         | 6.5   |  |                     |                   |       |                                  | +1   |
| T  | 2/4/2010          | 5.9   |  |                     |                   |       |                                  | +0.6 on SW striking nodal plane/+0.9 on NW striking nodal plane                      |

<sup>a</sup>Dates are given as month/day/year.

<sup>b</sup>Depends on rupture length.

144 and 2010  $M = 6.5$  earthquakes, the only three earthquakes  
145 with well-located aftershocks off the likely source fault.

## 146 6. Coulomb Stress Interactions Among Recent 147 $M \geq 5.9$ Earthquakes and Faults

148 [8] We calculate that the following interactions may have  
149 occurred among the 20  $M \geq 5.9$  earthquakes since 1976.

150 [9] 1. The source faults of eight earthquakes (earthquakes  
151 J, K, L, M, N, O, Q, and T) may have experienced Coulomb  
152 stress increases of  $\geq 0.6$  bar imparted by previous shocks  
153 (Table 3).

154 [10] 2. In six of those eight cases (J, K, L, N, Q, and T),  
155 the source fault ruptured less than 9 months after the imparted  
156 stress increase.

157 [11] 3. In five of the six short-term cases, the imparted  
158 Coulomb stress increase was  $\geq 0.9$  bar. The sixth is the stress  
159 change imparted by the January 2010  $M = 6.5$  Ferndale  
160 earthquake (S) to the source fault of the February 2010  $M_w =$   
161 5.9 earthquake (T); this stress increase was either 0.6 or  
162 0.9 bar.

163 [12] 4. The source fault of L (1992) experienced a Cou-  
164 lomb stress decrease of 2 bars imparted by E (1987), the one  
165 well-constrained case of an  $M \geq 5.9$  earthquake occurring  
166 despite a calculated  $\geq 0.6$  bar stress inhibition (Table 2).  
167 However, J (1992) imparted a Coulomb stress increase of  
168 3 bars to the source fault of L.

169 [13] 5. In all well-constrained  $\geq 0.2$  bar stress interactions  
170 between earthquakes that occurred within 4 years of each  
171 other, the second earthquake is promoted. The interaction  
172 between Q (2005) and R (2008) is calculated to be a 0.3 bar  
173 inhibition but is poorly constrained (Table S4 in the auxiliary  
174 material).<sup>1</sup>

<sup>1</sup>Auxiliary materials are available in the HTML. doi:10.1029/2009JB007117.

[14] 6. The epicenters of five  $M \geq 5.9$  earthquakes (I, L, N, P, and R) are very close to the inferred rupture areas of previous  $M \geq 5.9$  shocks (G, K, B, I, and D, respectively); these five stress interactions were strong but cannot be calculated reliably (Table 2).

**Table 3.** The Last Imparted  $\geq 0.5$  bar Stress Changes Before Occurrences of  $M \geq 5.9$  Earthquakes

| Earthquake | Last $\geq 0.5$ bar Coulomb Stress Change Imparted to Epicenter Prior to Earthquake |                                   |
|------------|---|-----------------------------------|
|            | Earthquake Imparting Stress Change  | Magnitude of Stress Change (bars) |
| A          | None  | -                                 |
| B          | None  | -                                 |
| C          | None  | -                                 |
| D          | None  | -                                 |
| E          | None  | -                                 |
| F          | None  | -                                 |
| G          | None  | -                                 |
| H          | None  | -                                 |
| I          | G (1991)  | Large but poorly constrained      |
| J          | H (1991)  | +1 (at epicenter) to +4           |
| K          | J (1992)  | +0.9                              |
| L          | J (1992)  | +3                                |
| M          | B (1980)  | +0.7                              |
| N          | M (1994)  | +3 to +10                         |
| O          | M (1994)  | +2 to +6                          |
| P          | I (1991)  | Large but poorly constrained      |
| Q          | P (2005)  | +1                                |
| R          | D (1984)  | Large but poorly constrained      |
| S          | None  | -                                 |
| T          | S (2010)  | +0.6/+0.9                         |

<sup>a</sup>Dates are given as month/day/year.

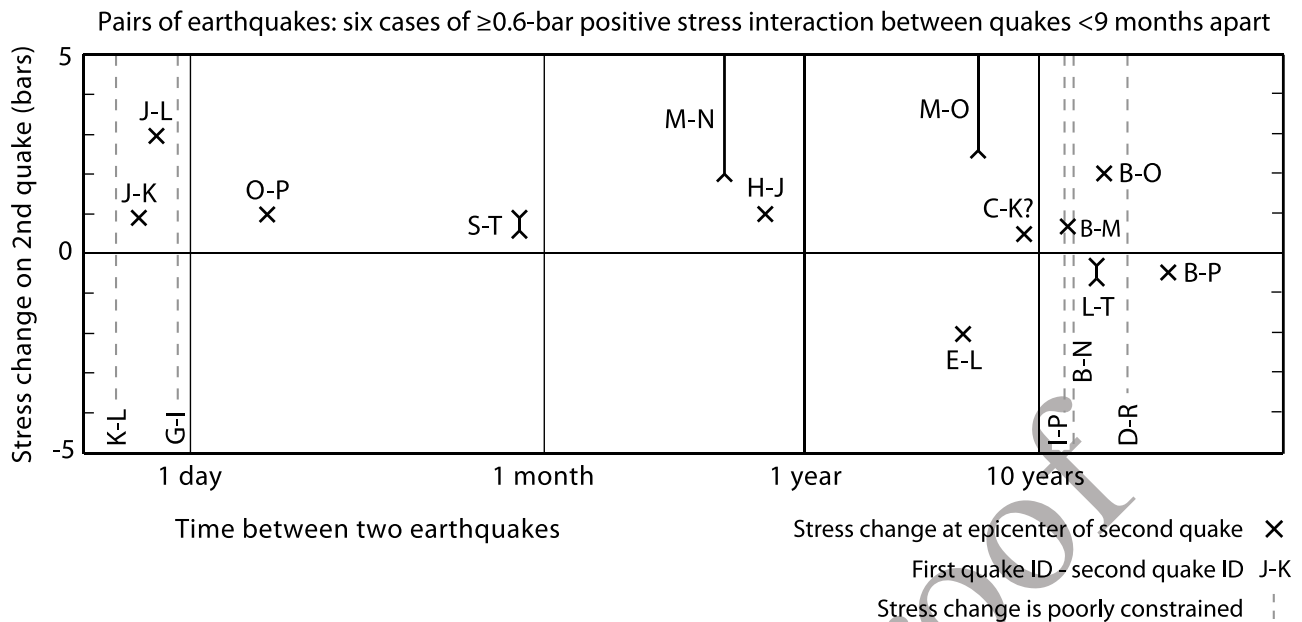


**Figure 3.** Given any two earthquakes, the first earthquake either promotes the failure of the second by Coulomb stress transfer, inhibits it, or has no effect. Shown here are all pairs of recent  $M \geq 5.9$  earthquakes in which the first earthquake is calculated to promote or inhibit the second by  $\geq 0.5$  bar (Table 2). Each cross represents a pair of two earthquakes. The horizontal axis is the time between the two earthquakes; the vertical axis is the calculated stress change at the epicenter of the second earthquake, given its orientation and rake. Note the six pairs of earthquakes less than 9 months apart in which the first promotes the second by  $\geq 0.6$  bar.

180 [15] 7. I (1991) and P (2005) may represent successive  
181 ruptures on a single fault, in which case the stress interaction  
182 between them would be strong and positive (Figure 1). This  
183 may also be true of B (1980) and N (1995).

184 [16] 8. The other nine  $M \geq 5.9$  shocks (A, B, C, D, E, F,  
185 G, H, S) did not occur at the sites of  $\geq 0.5$  bar Coulomb  
186 stress interactions imparted by previous earthquakes since  
187 1976 (Table 3), though F may have promoted G by up to  
188 0.3 bar (Table S4).

189 [17] 9. We calculate that the 1980  $M_w = 7.3$  Trinidad  
190 earthquake (B) imparted a Coulomb stress decrease to much  
191 of the southern Gorda zone. The locations of  $M \geq 5.9$   
192 earthquakes in this area before 1995 (E, F, G, and I) are  
193 consistent with the few regions where stress was not  
194 decreased in 1980 (Figure 3, Figure 4).

195 [18] 10. Stress changes imparted by B are also consistent  
196 with a band of off-fault aftershocks on and around the  
197 Mendocino Fault Zone.

### 198 6.1. Stress Changes Imparted by the 9 November 1980, 199 $M_w = 7.3$ , Earthquake (B)

#### 200 6.1.1. Aftershocks

201 [19] The 1980 Trinidad earthquake (B) produced a distinct  
202 elbow-shaped aftershock pattern that included both a main  
203 NE trending band of aftershocks on the rupture and a sep-  
204 arate WNW trending cluster to the south [Eaton, 1987; Hill  
205 *et al.*, 1990] (also relocations by J.P. Eaton using phase data  
206 from TERA Corporation and NCSN) (Figure 4). The  
207 aftershock clusters are hereafter referred to by the number-  
208 ing system used in Figures 2 (earthquake A) and 4. The off-  
209 fault cluster south of the rupture, labeled “3” in Figures 2  
210 and 4, trends  $285^\circ$  and initially follows the right-lateral

Mendocino Fault Zone but becomes misaligned west of 211  
125.5°W longitude as the fault zone curves due west; the 212  
aftershocks taper off at  $126^\circ$ W, 20 km north of the fault 213  
zone. The seismicity between  $125.5^\circ$ W and  $126^\circ$ W is either 214  
on the Mendocino Fault Zone (with errors in location) or on 215  
left-lateral faults just to the north. Our source model for the 216  
1980 main shock increases Coulomb stress on both the 217  
Mendocino Fault Zone between  $125^\circ$ W and  $125.8^\circ$ W and 218  
nearby left-lateral faults between  $125.5^\circ$ W and  $126^\circ$ W. 219  
Thus, seismicity between  $125.8^\circ$ W and  $126^\circ$ W is inconsis- 220  
tent with calculated stress changes if it is on the Mendocino 221  
Fault Zone, but the rest of cluster 3 (>70% of it) is consistent 222  
with stress changes regardless of what fault system it 223  
occurred on. If seismicity between  $125.8^\circ$ W and  $126^\circ$ W is 224  
on left-lateral faults, the entire cluster is consistent with 225  
calculated stress changes. 226

[20] These findings assume that the 1980 rupture did not 227  
extend to the Mendocino Fault Zone and is defined only by 228  
clusters 1 and 2 to the northeast. If the rupture extended 229  
southwest to cluster 3, Coulomb stress would have been 230  
increased on the Mendocino Fault Zone between  $125^\circ$ W and 231  
 $126^\circ$ W, consistent with some of cluster 3, though after- 232  
shocks between  $125.5^\circ$ W and  $126^\circ$ W would be on the 233  
rupture. The calculated stress increase between  $125^\circ$ W and 234  
 $125.8^\circ$ W on the Mendocino Fault Zone is robust. 235

[21] In addition to aftershocks on the rupture and the 236  
Mendocino Fault Zone, Eaton [1987] and Hill *et al.* [1990] 237  
show a localized cluster at  $\leq 10$  km depth 25 km east of the 238  
main  $N50^\circ$ E trend (“4” in Figures 2, earthquake A, and 4). 239  
This cluster may be on a separate area of slip in the 1980 240  
main shock, a left-lateral fault parallel to the rupture, the 241  
Cascadia subduction zone (the megathrust interface would 242

Source earthquake: November 8, 1980,  $M_w=7.3$  (B)  
 Receivers: Mendocino Fault Zone, Cascadia subduction zone, and left-lateral faults

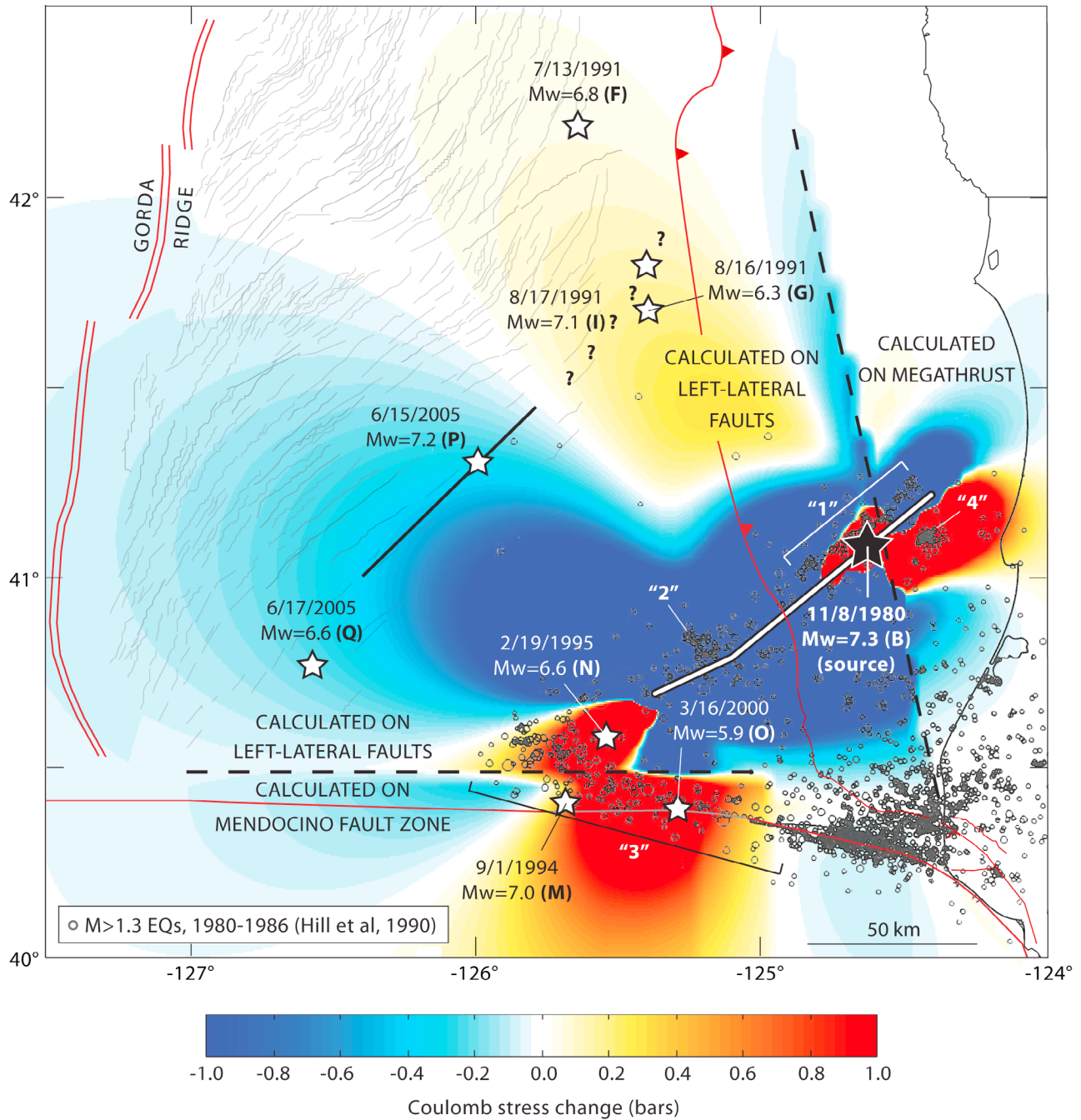


**Figure 4.** Coulomb stress changes imparted by the 1980  $M_w = 7.3$  earthquake (B) to a matrix of faults representing the Mendocino Fault Zone, the Cascadia subduction zone, and NE striking left-lateral faults in the Gorda zone. The Mendocino Fault Zone is represented by right-lateral faults whose strike rotates from  $285^\circ$  in the east to  $270^\circ$  in the west; Cascadia is represented by reverse faults striking  $350^\circ$  and dipping  $9^\circ$ ; faults in the Gorda zone are represented by vertical left-lateral faults striking  $45^\circ$ . The boundary between the left-lateral “zone” and the reverse “zone” in the fault matrix is placed at the 6 km depth contour on Cascadia, approximated by extending the top edge of the *Oppenheimer et al.* [1993] model for the 1992 Cape Mendocino earthquake (J). Calculation depth is 5 km. The numbered brackets are groups of aftershocks from *Hill et al.* [1990].

243 be at 7–8 km depth at the location of the cluster), or faults  
244 within the overriding North American plate (R. C. McPherson,  
245 personal communication, 2010). Our model for the 1980  
246 earthquake increases Coulomb stress on the Cascadia sub-  
247 duction zone in the area of cluster 4 and decreases stress  
248 elsewhere on the megathrust, so if cluster 4 is on the  
249 megathrust, it is consistent with stress changes imparted by  
250 the 1980 earthquake.

#### 251 6.1.2. Subsequent $M \geq 5.9$ Earthquakes

252 [22] Two  $M \geq 5.9$  earthquakes ruptured the Mendocino  
253 Fault Zone between 125°W and 125.8°W after 1980: a  
254  $M_w = 7.0$  earthquake at 125.7°W in 1994 (M) and a  $M_w =$   
255 5.9 earthquake at 125.3°W in 2000 (O). Our source model  
256 for B imparts Coulomb stress increases of 0.7 and 2.0 bars  
257 to the epicenters of M and O, respectively (Figure 4).

258 [23] In 1995, an  $M_w = 6.6$  left-lateral earthquake (N)  
259 struck near the southwest end of the inferred rupture area of  
260 B. Because of uncertainties in locations and rupture areas,  
261 the stress interaction between these two earthquakes is not  
262 well constrained. However, the location of N suggests that  
263 these earthquakes may represent successive ruptures on one  
264 fault, in which case the stress interaction between them  
265 would have been strong and positive, as in the case of 20th  
266 century earthquakes on the North Anatolian Fault [Stein  
267 *et al.*, 1997].

268 [24] Excluding faults to the southwest, we calculate that B  
269 decreased Coulomb stress on most left-lateral faults in the  
270 southern Gorda deformation zone, producing a “stress  
271 shadow.” Four  $M \geq 5.9$  left-lateral earthquakes occurred in  
272 the Gorda zone between 1980 and 1994: a  $M_w = 6.0$   
273 earthquake at Cape Mendocino in 1987 (E) and three  $M \geq$   
274 6.3 earthquakes to the north of the 1980 rupture in the  
275 summer of 1991 (F, G, and I). We calculate that these  
276 shocks all occurred outside of the stress shadow of B: the  
277 source fault of E experienced no stress change in 1980, and  
278 left-lateral faults in the region in which F, G and I occurred  
279 experienced a  $\leq 0.2$  bar stress increase in 1980. The locations  
280 of  $M \geq 5.9$  left-lateral earthquakes until at least 1995 were  
281 thus consistent with calculated stress changes imparted by  
282 B, and if N (1995) occurred on the same fault as B, that  
283 stress interaction was positive as well. The first  $M \geq 5.9$   
284 earthquake to definitely occur within the calculated 1980  
285 stress shadow was the 2005  $M_w = 7.2$  shock (P).

#### 286 6.2. Stress Changes Imparted by Earthquake C (1983) 287 to K and L (1992)

288 [25] The 24 August 1983  $M_w = 6.1$  earthquake (C)  
289 occurred near the future site of the 25 April 1992  $M_w = 6.9$   
290 Cape Mendocino earthquake (J) and its two deep  $M_w = 6.5$   
291 (K) and  $M_w = 6.6$  (L) aftershocks. Our model for C imparts  
292 a negligible Coulomb stress change to the source fault of  
293 J but increases stress by 0.5 bar at the epicenter of K and  
294 decreases stress by 0.4 bar at the epicenter of L (Figure 5c).  
295 The interactions with K and L are dependent on the rupture  
296 length of C, so they are poorly constrained.

#### 297 6.3. Stress Changes Imparted by E (1987) to K and L 298 (1992)

299 [26] Our model for the 31 July 1987  $M_w = 6.0$  Cape  
300 Mendocino earthquake (E) decreases Coulomb stress by 0.2  
301 and 2 bars at the epicenters of K and L (1992), respectively  
302 (Figure 5c).

#### 6.4. Stress Changes Imparted by the 1991 Honeydew Earthquake (H) to the 1992 $M_w = 6.9$ Cape Mendocino Shock (1992)

[27] Our model for the 17 August 1991  $M_w = 6.1$  Honeydew  
earthquake (H) increases Coulomb stress by  $\geq 1$  bar on the  
southern part of the *Oppenheimer et al.* [1993] rupture  
surface for the 25 April 1992  $M_w = 6.9$  Cape Mendocino  
earthquake (J), including a stress increase of 1 bar at the  
1992 epicenter.

#### 6.5. Stress Changes Imparted by I (1991) to P (2005)

[28] The location error for the 17 August 1991  $M_w = 7.1$   
earthquake (I) is too great for its stress interaction with the  
15 June 2005  $M_w = 7.2$  earthquake (P) to be calculated  
reliably. When compared to the *Chaytor et al.* [2004] faults,  
the NEIC locations for these two earthquakes suggest that  
they may represent successive ruptures on a single fault  
(Figure 1), in which case the stress interaction between them  
would have been strong and positive. If they occurred on  
parallel but separate faults, the stress interaction could have  
been either positive or negative depending on their rupture  
lengths. Earthquakes A (1976) and B (1980) imparted  
Coulomb stress decreases to the source fault of P; these may  
have affected the timing of P and may be linked to the  
14 year intervening period between I and P.

#### 6.6. Stress Changes Imparted by the 25 April 1992, $M_w = 6.9$ , Cape Mendocino Earthquake (J)

##### 6.6.1. Faults Parallel to Source

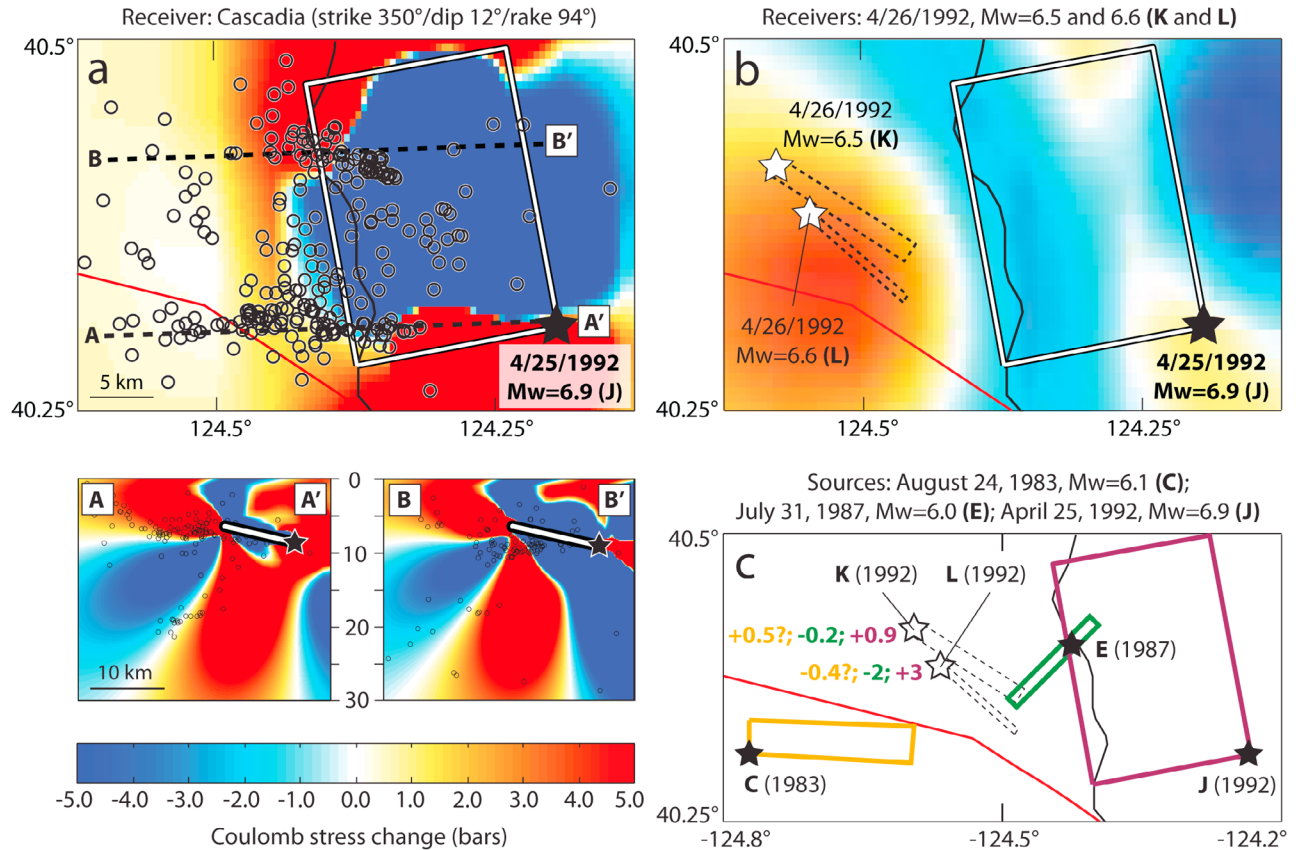
[29] Small aftershocks of this earthquake are mainly con-  
centrated in two WNW trending linear clusters (Figure 5). If  
these are taken to represent the northern and southern edges  
of the rupture plane, the *Oppenheimer et al.* [1993] model is  
aligned with the southern cluster but somewhat misaligned  
with the northern cluster. Similarly, Coulomb stress changes  
imparted to thrust faults are consistent with the southern  
aftershock cluster but only partially consistent with the  
northern cluster (Figure 5a).

##### 6.6.2. Stress Changes Imparted to K and L (26 April 1992, $M_w = 6.5$ and 6.6)

[30] The  $M_w = 6.9$  Cape Mendocino earthquake (J) was  
followed 12 and 15 h later by  $M_w = 6.5$  (K) and  $M_w = 6.6$   
(L) aftershocks at 15–25 km depth. Our source model for  
the  $M_w = 6.9$  shock increases Coulomb stress by 0.9 bar at  
the epicenter of K and by 3 bars at the epicenter of L  
(Figure 5b). The stress changes imparted to the epicenters  
of the two aftershocks by earthquakes in 1983 (C) and  
1987 (E) may explain why K occurred first even though L  
was more strongly promoted by J (Figure 5c).

#### 6.7. Stress Changes Imparted by the 1994, $M_w = 7.0$ , Mendocino Fault Zone Earthquake (M) to N (1995) and O (2000)

[31] To account for uncertainties in the location of the  
1994  $M_w = 7.0$  Mendocino Fault Zone earthquake (M), we  
made one source model with the NEIC epicenter at the  
centroid (model 1) and one with the epicenter at the west end  
(model 2). Model 1 increases Coulomb stress by 3–6 bars at  
the epicenter of the 1995  $M_w = 6.6$  southern Gorda zone  
shock (N), and increases stress by 2–3 bars at the epicenter  
of the 2000  $M_w = 5.9$  earthquake on the Mendocino Fault  
Zone (O) (Figure 6). Model 2 for the 1994 earthquake

Source: April 25, 1992,  $M_w=6.9$ , Cape Mendocino, CA (J)

**Figure 5.** (a) Coulomb stress changes imparted by the 1992  $M_w = 6.9$  Cape Mendocino earthquake (J) to the Cascadia subduction zone. Calculation depth is 8 km. Open circles are *Waldhauser and Schaff's* [2008] earthquake locations for 25 April 1992 to 2 May 1992, 0–15 km depth. Seismicity data were cut off at 15 km depth to prevent interference from aftershocks of K and L. Cross section A-A' includes seismicity between 40.24°N and 40.36°N. Cross section B-B' includes seismicity between 40.36°N and 40.48°N. (b) Coulomb stress changes imparted by the 1992  $M_w = 6.9$  earthquake (J) to  $M_w = 6.5$  and  $M_w = 6.6$  shocks the next day (K and L). Stress change is resolved on the average of the orientations of K and L (strike 127°/dip 90°/rake 180°). Calculation depth is 21.5 km. (c) Calculated Coulomb stress changes imparted by  $M \geq 5.9$  shocks in 1983, 1987, and 1992 (C, E, and J) to the epicenters of K and L. The series of three colored numbers represent stress changes imparted by C, E, and J, respectively.

362 increases stress by 4–10 bars at the epicenter of N and  
 363 increases stress by 6 bars at the epicenter of O. The stress  
 364 interaction between earthquakes B (1980) and N is strong  
 365 but poorly constrained, so the combined stress change  
 366 imparted to the source fault of N by B and M is unknown.  
 367 As M occurred much closer in time to N, its stress effect  
 368 may have been more important than that of B. More robust  
 369 is the observation that both B and M imparted >1 bar stress  
 370 increases to the epicenter of O; this is our best constrained  
 371 interaction on a >10 year timescale.

### 372 6.8. Stress Changes Imparted by P (15 June 2005, 373 $M_w = 7.2$ ) to Q (17 June 2005, $M_w = 6.6$ )

374 [32] The G. Shao and C. Ji (Preliminary result for rupture  
 375 process of June 15, 2005  $M_w = 7.2$  northern California  
 376 earthquake, 2005, available at [http://www.geol.ucsb.edu/](http://www.geol.ucsb.edu/faculty/ji/big_earthquakes/2005/06/smooth/northernca.html)  
 377 [faculty/ji/big\\_earthquakes/2005/06/smooth/northernca.html](http://www.geol.ucsb.edu/faculty/ji/big_earthquakes/2005/06/smooth/northernca.html),  
 378 hereafter cited as Shao and Ji, 2005) source model for the

15 June 2005  $M_w = 7.2$  earthquake (P) imparts a Coulomb  
 stress increase of 1 bar to the epicenter of a  $M_w = 6.6$  shock  
 to the southwest which occurred 51 h later (Q) (Figure 7).  
 These earthquakes may represent successive ruptures on a  
 single fault; the orientations of local *Chaytor et al.* [2004]  
 faults indicate that the NEIC epicenter for Q would have  
 to be incorrect by ~10 km for the two earthquakes to be on  
 the same fault.

### 6.9. Stress Changes Imparted by the 10 January 2010, $M = 6.5$ Earthquake (S)

#### 6.9.1. Aftershocks and Cascadia Subduction Zone

[33] The 10 January 2010,  $M = 6.5$ , earthquake had an  
 L-shaped aftershock pattern, with a main N50°–55°E  
 on-fault trend and a separate N45°W trend at the southwest  
 end of the rupture (Figure 8). We calculate that the main  
 shock increased Coulomb stress on NW striking faults to the  
 southwest, somewhat consistent with the NW trending off-

Source earthquake: September 1, 1994,  $M_w=7.0$ , Mendocino Fracture Zone (M)  
 Receivers: Mendocino Fracture Zone and NE-striking left-lateral faults

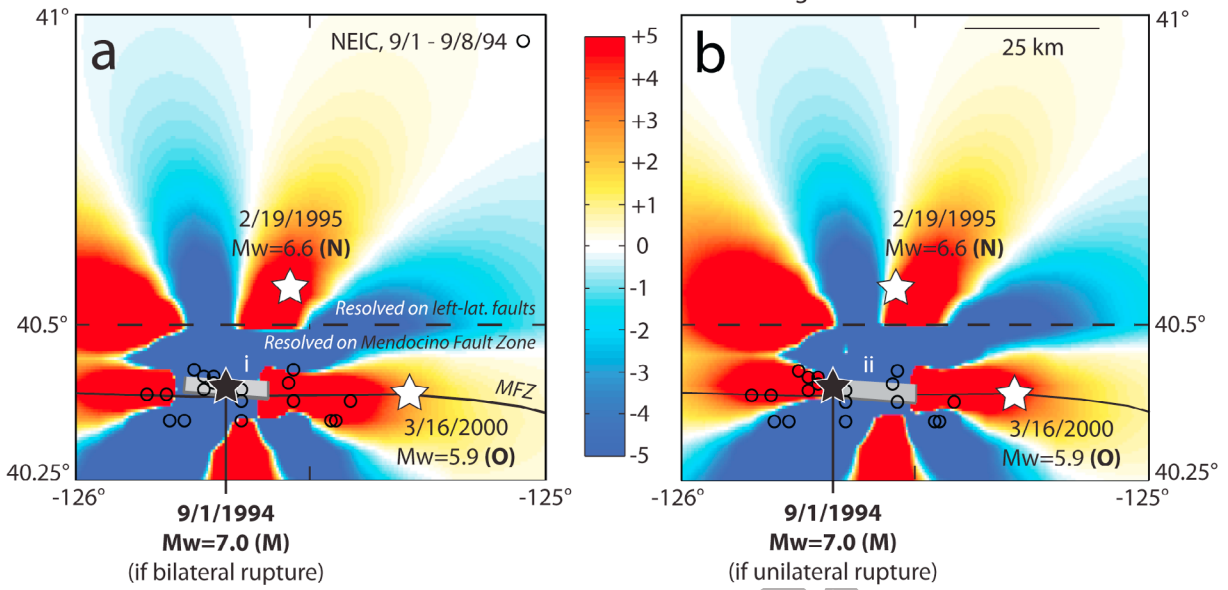


**Figure 6.** Coulomb stress changes imparted by our models of (a) a bilateral rupture and (b) a unilateral eastward rupture for the 1994  $M_w = 7.0$  Mendocino Fault Zone earthquake to the epicenters of the 1995  $M_w = 6.6$  southern Gorda zone earthquake (N) and the 2000  $M_w = 5.9$  Mendocino Fault Zone earthquake (O). Calculation depth is 5 km.

Source earthquake: June 15, 2005,  $M_w=7.2$  (P)  
 Receiver: June 17, 2005,  $M_w=6.6$  (Q) (strike 202°/dip 89°/rake -8°)

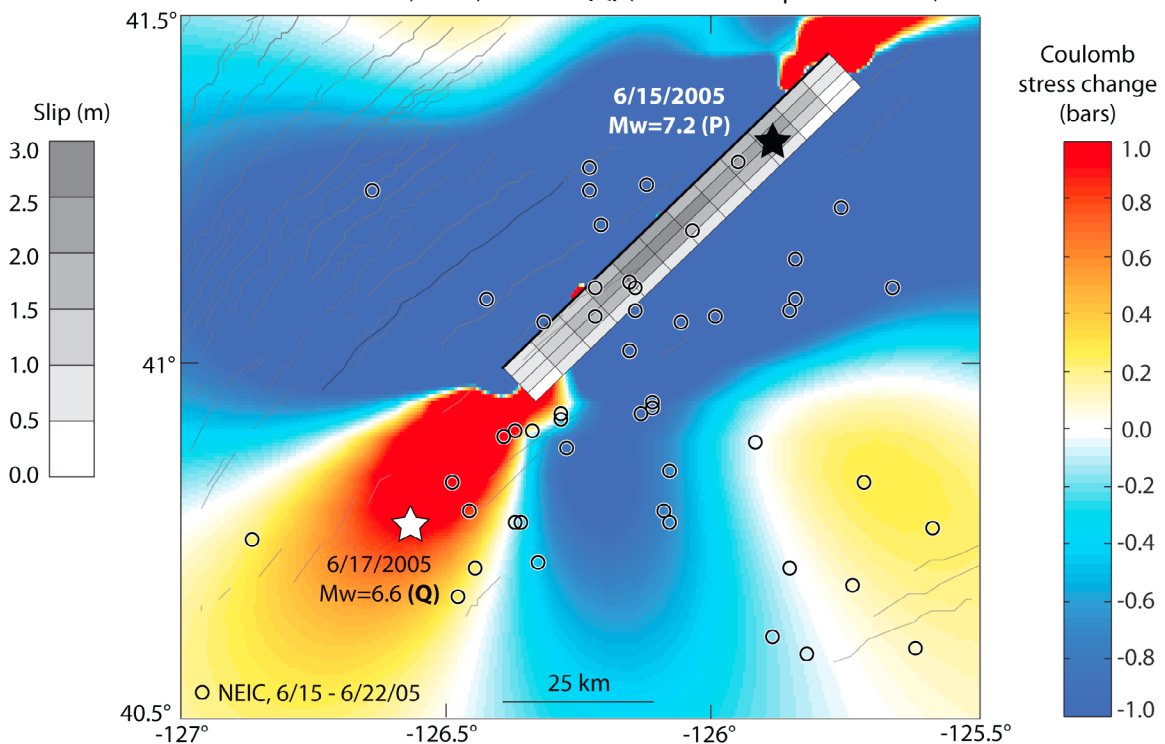


**Figure 7.** Coulomb stress changes imparted by the Shao and Ji (2005) variable slip model for the 15 June 2005  $M_w = 7.2$  earthquake (P) to the epicenter of the 17 June 2005  $M_w = 6.6$  earthquake (Q). Calculation depth is 10 km.

Source earthquake: January 10, 2010,  $M=6.5$  (S)  
 Receivers: February 4, 2010  $M_w=5.9$  quake (T), nodal plane 2 (strike 306°/dip 85°/rake -169°),  
 and Cascadia subduction zone

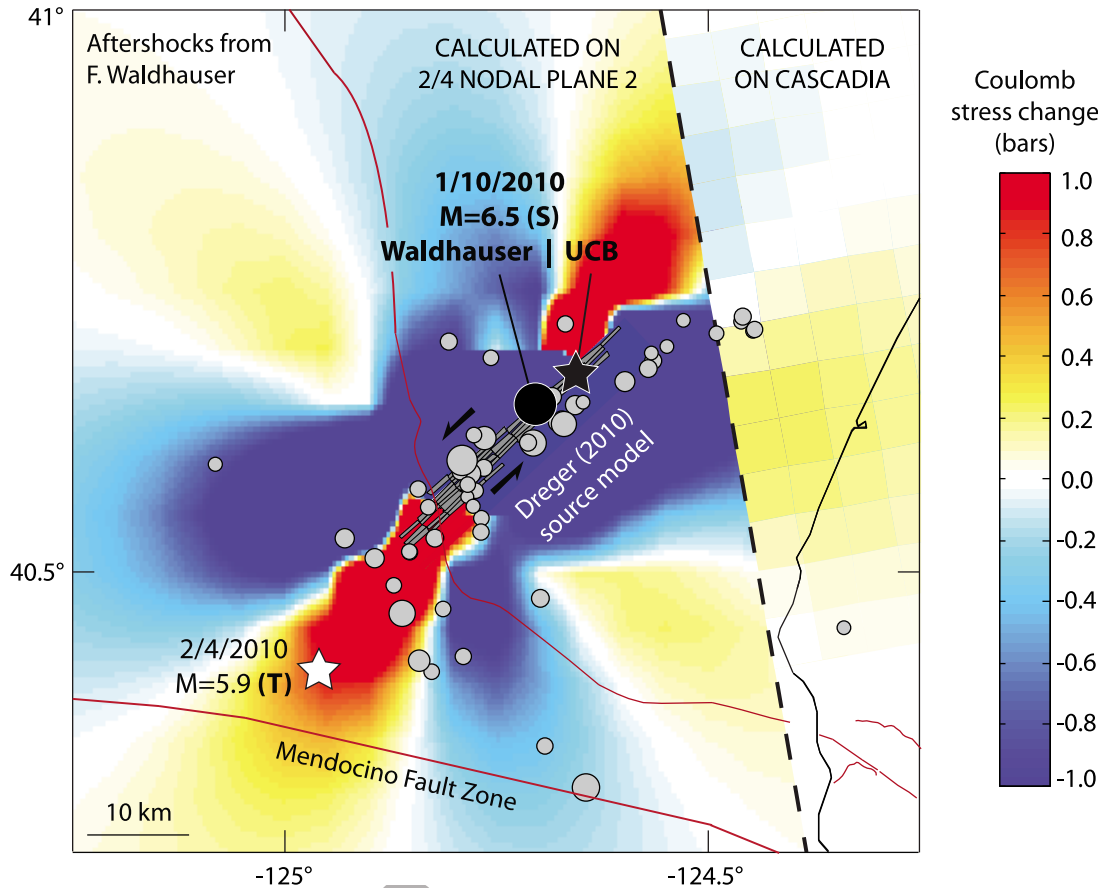


**Figure 8.** Coulomb stress changes imparted by the D. Dreger (unpublished report, 2010) model for the January 2010  $M = 6.5$  shock (S) to nearby faults. East of the dashed line, stress changes are resolved on the Cascadia subduction zone, represented by a northward extension of the *Oppenheimer et al.* [1993] rupture plane for the 1992  $M_w = 6.9$  Cape Mendocino earthquake. West of the dashed line, stress changes are resolved on the NW striking nodal plane for the February 2010  $M_w = 5.9$  earthquake (T) at a depth of 23.6 km.

396 fault aftershock cluster. In addition, the main shock imparted  
 397 a 0.2 bar Coulomb stress increase to the Cascadia subduc-  
 398 tion zone at 6–7 km depth southwest of Eureka, California.

### 399 6.9.2. Stress changes Imparted to the 4 February 2010 400 $M_w = 5.9$ Earthquake (T)

401 [34] The 4 February 2010  $M_w = 5.9$  earthquake (T)  
 402 occurred on either a NW or SW striking fault; its aftershocks  
 403 do not define a linear trend. We find that the January  $M =$   
 404 6.5 earthquake imparted Coulomb stress increases of 0.9 bar  
 405 to the NW striking nodal plane for T and 0.6 bar to the SW  
 406 striking nodal plane (Figure 8 and Table 2).

### 407 6.10. Other Cases of Large but Poorly Constrained 408 Coulomb Stress Transfer

409 [35] Two other  $M \geq 5.9$  earthquakes occurred very close to  
 410 the rupture areas of previous earthquakes: L occurred close  
 411 to K and R occurred close to D (Table 2). In these cases,  
 412 possible errors in locations and rupture areas exceed the

distances between the two earthquakes, so these stress 413  
 interactions, although strong, cannot be calculated reliably. 414

## 7. Location-Randomized Control Tests 415

[36] Given a random set of 20 independent but closely 416  
 spaced  $M \geq 5.9$  earthquakes, how many  $\geq 0.6$  bar Coulomb 417  
 stress interactions would appear to occur between earth- 418  
 quakes less than 9 months apart? We run three control tests 419  
 in which we assign the recent  $M \geq 5.9$  earthquakes random 420  
 epicenter locations between 40.25°N and 42.5°N latitude 421  
 and between 124°W and 127°W longitude, an area in which 422  
 all of the recent  $M \geq 5.9$  earthquakes occurred (Figure S1). 423  
 The orientations of the source models with respect to the 424  
 epicenters are kept the same as in the actual 1976–2010 425  
 sequence, except that if two location-randomized source 426  
 models intersect, we rotate one of the two models 180° 427  
 about its epicenter. The magnitudes, rupture dimensions and 428

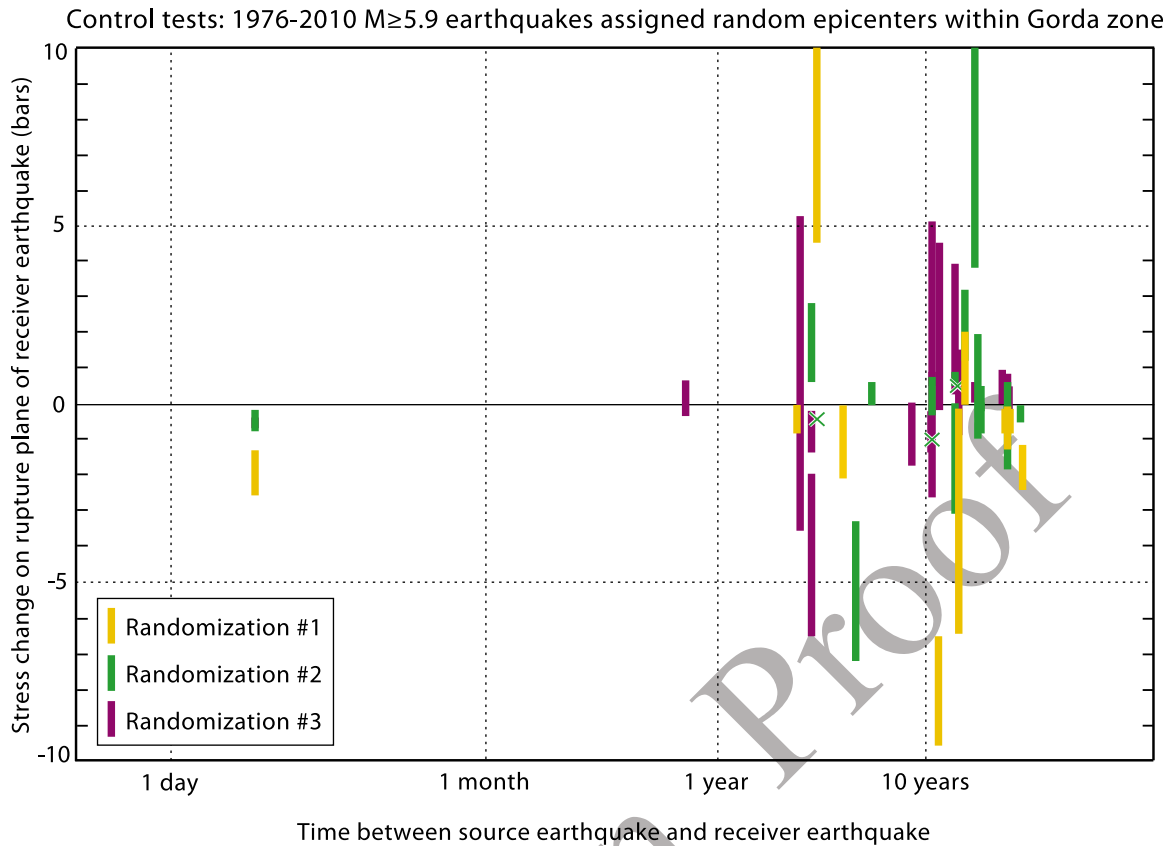


**Figure 9.** Coulomb stress changes of magnitude  $\geq 0.5$  bars between  $M \geq 5.9$  earthquakes in three location-randomized control tests. The crosses and axes serve the same purposes as in Figure 3. Note the absence of cases of  $\geq 0.6$  bar promotion among pairs of earthquakes separated by  $< 1$  year, compared to six cases of  $\geq 0.6$  bar short-term promotion in Figure 3.

429 orientations, and dates of the earthquakes are the same as in  
 430 the actual sequence. We run this procedure three times to  
 431 generate three dissimilar, essentially random distributions of  
 432 the recent  $M \geq 5.9$  earthquakes.  
 433 [37] Four earthquakes in set 2 and five earthquakes in  
 434 set 3 are nominally promoted  $\geq 0.6$  bar by previous shocks,  
 435 suggesting that it is possible for as many as eight  $M \geq 5.9$   
 436 shocks in a set of 20 to appear to be promoted  $\geq 0.6$  bar by  
 437 previous earthquakes (Figure 9 and Tables S1–S3). How-  
 438 ever, the control tests do not reproduce the high number of  
 439  $\geq 0.6$  bar positive Coulomb interactions between earthquakes  
 440  $< 9$  months apart: only one such case is observed between

the three control tests, compared to six in the actual 1976– 441  
 2010 sequence (Table 4). 442

**8. Coulomb Stress Changes Imparted by the 1906 443  
 San Francisco Earthquake 444**

[38] The great 1906 earthquake ruptured the San Andreas 445  
 Fault to the Mendocino Triple Junction and may have imparted 446  
 long-lasting stress changes to nearby faults (Figure 10). We 447  
 use the *Song et al.* [2008] slip model; the northernmost 448  
 40 km of this model deviates by 5–10 km from the San 449  
 Andreas Fault trace in the USGS Quaternary Fault and Fold 450

t4.1 **Table 4.** Comparison of Coulomb Stress Interactions in Actual 1976–2010 Sequence and Control Tests

| t4.2  | Set of $M \geq 5.9$ Earthquakes                      | Actual 1976–2010 Sequence | Control set 1 | Control Set 2 | Control Set 3 |
|-------|--|---------------------------|---------------|---------------|---------------|
| t4.3  | Number of earthquakes promoted $\geq 0.6$ bar        | 8                         | 1             | 4             | 5             |
| t4.4  | On $< 9$ month timescale                             | (6)                       | -             | -             | (1)           |
| t4.5  | Number of earthquakes inhibited $\geq 0.6$ bar       | 1                         | 7             | 5             | 4             |
| t4.6  | On $< 9$ month timescale                             | -                         | (2)           | (1)           | -             |
| t4.7  | Number of earthquakes promoted and inhibited         | -                         | -             | -             | 3             |
| t4.8  | $\geq 0.6$ bar on different sections of source fault | -                         | -             | -             | -             |
| t4.9  | On $< 9$ month timescale                             | -                         | -             | -             | -             |
| t4.10 | Total  | 15                        | 8             | 9             | 12            |

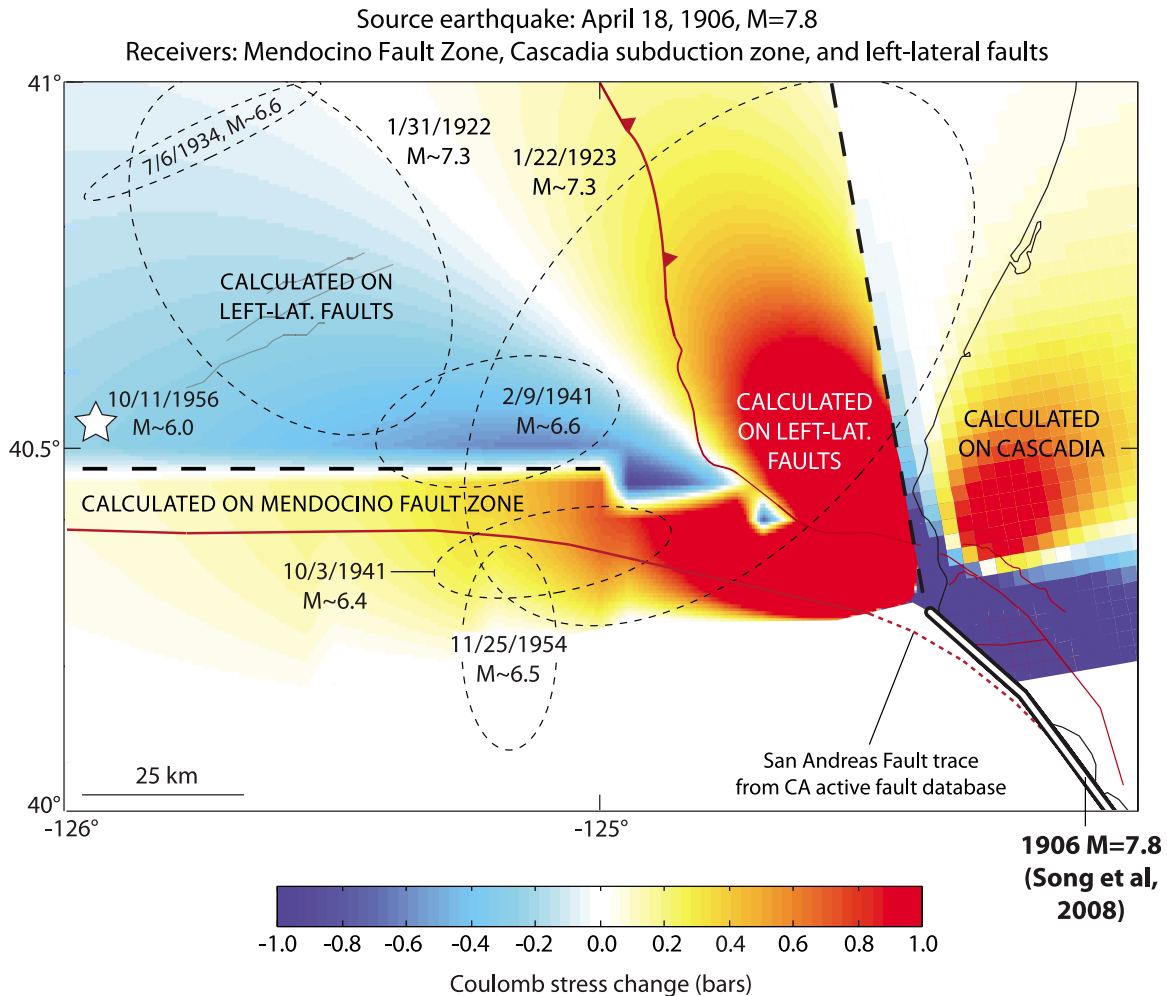


**Figure 10.** Coulomb stress changes imparted by the 1906 San Andreas earthquake to the Mendocino Fault Zone, the Cascadia megathrust, and northeast striking left-lateral faults within the Gorda zone. The fault matrix is the same as that used in Figure 4, except that the Cascadia subduction zone is represented by a northward and downdip extension of the *Oppenheimer et al.* [1993] rupture plane, as in Figure 8. Ellipses are 95% confidence contours for 1922–1961  $M > 6$  earthquakes from D. I. Doser (manuscript in preparation, 2010). Calculation depth is 5 km.

451 Database (Figure 10). We calculate that the 1906 earthquake  
 452 increased stress on the Mendocino Fault Zone and both  
 453 increased and decreased stress on Gorda zone left-lateral  
 454 faults depending on location. These stress changes may be  
 455 consistent with the locations of large offshore earthquakes in  
 456 1923, 1941 and 1954, but are inconsistent with other shocks  
 457 in 1922, 1934, 1941 and 1956 (D. I. Doser, manuscript in  
 458 preparation, 2010). In addition, the *Song et al.* [2008] source  
 459 increases stress by  $>1$  bar on the Cascadia megathrust north  
 460 of  $40.35^\circ\text{N}$  latitude and decreases stress on the megathrust  
 461 south of it. This is roughly consistent with the results of  
 462 *Goldfinger et al.* [2008], who used the *Thatcher et al.* [1997]  
 463 model for the 1906 earthquake.

## 464 9. Dynamic Triggering?

465 [39] In 1991, a  $M_w = 6.3$  shock offshore Crescent City,  
 466 California (G), was followed 21 h later by the  $M_w = 6.1$   
 467 Honeydew earthquake (H) 200 km to the southeast, well  
 468 outside the range of static stress interaction (Figure 1).

Dynamic interaction between these two earthquakes is 469  
 possible, although H is in a direction perpendicular to the 470  
 northeast/southwest rupture propagation of G. No seismicity 471  
 is observed at the future site of H during the 21 h between 472  
 the two earthquakes. 473

## 474 10. Discussion

### 475 10.1. Influence of Coulomb Stress Changes on $M \geq 5.9$ Earthquakes

[40] Control tests show that it is possible for eight  $M \geq 5.9$  477  
 shocks in a random set of 20 to appear to be promoted  $\geq 0.6$  478  
 bar by previous earthquakes in the set, but highly unlikely 479  
 for six earthquakes to appear to be promoted  $\geq 0.6$  bar by 480  
 earthquakes  $<9$  months before. This indicates that the cal- 481  
 culated Coulomb stress promotions of earthquakes J, K, L, 482  
 N, Q, and T in the 1976–2010 Gorda zone sequence, if they 483  
 are correct, are unlikely to be an apparent effect, and that 484  
 imparted Coulomb stress changes probably influenced the 485  
 timing and location of these six earthquakes. Only stress 486

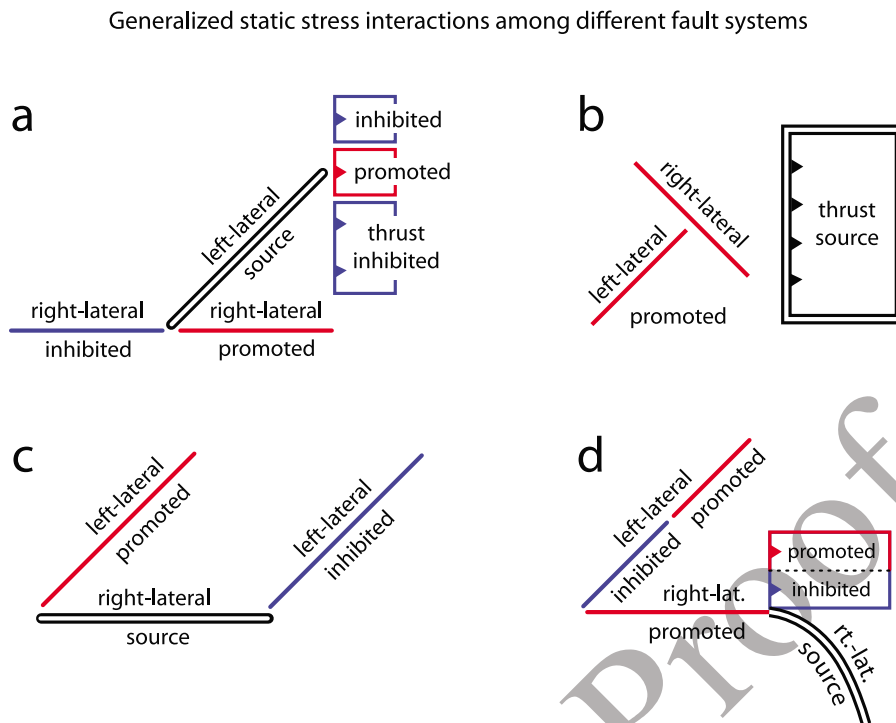


**Figure 11.** Generalized Coulomb stress interactions between faults of different orientations and rakes based on observations in the Gorda deformation zone.

487 interactions on <1 year timescales stand out from the ran-  
 488 domized control tests, suggesting that static stress change  
 489 may typically influence seismicity for periods on the order  
 490 of a year in the Gorda deformation zone, consistent with the  
 491 observations of *Harris et al.* [1995] in southern California.  
 492 However, the absence of  $M \geq 5.9$  earthquakes in the stress  
 493 shadow of the 1980  $M_w = 7.3$  earthquake (B) until at least  
 494 1995 suggests that the longevity of static stress changes may  
 495 increase for the largest main shocks, perhaps because they  
 496 trigger viscoelastic deformation that can eventually amplify  
 497 the coseismic stress changes [*Chan and Stein, 2009*].

#### 498 10.2. Promotion of Aftershocks off the Source Fault

499 [41] Most of the 1980  $M_w = 7.3$  earthquake's elbow-  
 500 shaped aftershock pattern can be correlated with Coulomb  
 501 stress changes imparted to the right-lateral Mendocino Fault  
 502 Zone and nearby left-lateral faults. Stress changes imparted  
 503 by the January 2010 Ferndale earthquake are also somewhat  
 504 consistent with a band of aftershocks perpendicular to the  
 505 source. This suggests that Coulomb stress changes can  
 506 trigger small earthquakes on faults nonparallel to the source,  
 507 in addition to promoting large subsequent earthquakes.

#### 508 10.3. Generalized Coulomb Interactions Among 509 Different Fault Systems

510 [42] Observations of stress interactions between faults in  
 511 this region can be applied to triple junctions and similar  
 512 tectonic settings elsewhere (Figure 11). An earthquake on a  
 513 northeast striking left-lateral fault increases Coulomb stress  
 514 on right-lateral faults to the south but decreases stress on  
 515 right-lateral faults to the southwest, and a strike-slip earth-  
 516 quake in a subducting slab increases stress on a localized

section of the subduction zone above it (Figure 11a). An  
 517 earthquake on a north striking thrust fault increases Coulomb  
 518 stress on northeast striking left-lateral faults and northwest  
 519 striking right-lateral faults to the west (Figure 11b). An  
 520 earthquake on an east striking right-lateral fault increases  
 521 stress on left-lateral faults north of the rupture but decreases  
 522 stress on left-lateral faults to the northeast (Figure 11c). A  
 523 large earthquake on the northernmost San Andreas increases  
 524 stress on the eastern Mendocino Fault Zone and both  
 525 increases and decreases stress on the Cascadia megathrust  
 526 and Gorda zone left-lateral faults depending on location  
 527 (Figure 11d).  
 528

## 529 11. Conclusion

[43] We find that  $\geq 0.6$  bar Coulomb stress increases  
 530 probably influenced the timing and location of at least 6 of  
 531 20 recent  $M \geq 5.9$  earthquakes in the Gorda deformation  
 532 zone. The occurrence of several other  $M \geq 5.9$  earthquakes  
 533 may have been indirectly influenced by the stress shadow  
 534 imparted by the 1980  $M_w = 7.3$  earthquake, which may have  
 535 lasted until 1995 or later. Stress changes imparted by the  
 536 1980 earthquake are also consistent with off-fault after-  
 537 shocks on and around the right-lateral Mendocino Fault  
 538 Zone. These findings indicate that earthquake interaction by  
 539 static stress transfer can occur among faults of differing  
 540 orientations, rakes and depths. Static stress changes may  
 541 affect seismicity for periods on the order of 1 year in the  
 542 Gorda zone, and perhaps for over a decade in the case of  
 543  $M > 7.2$  earthquakes. The generalized static stress interac-  
 544 tions derived from our observations of the 1976–2010  
 545

546 Gorda zone sequence may be applied to seismicity at similar  
547 tectonic settings elsewhere.

## 548 Appendix A

### 549 A1. Rupture Models

#### 550 A1.1. Earthquake A: 26 November 1976, $M_w = 6.7$ , 551 off Trinidad, California

552 [44] The Global CMT focal mechanism and the *Chaytor*  
553 *et al.* [2004] faults suggest that this earthquake occurred  
554 on a NE striking left-lateral fault. NEIC aftershock locations  
555 are inconsistent with this orientation, but aftershock loca-  
556 tions from the TERA Corporation [Smith *et al.*, 1982; R. C.  
557 McPherson, personal communication, 2010] are consistent  
558 with a NE striking fault plane and somewhat consistent with  
559 the NEIC main shock location. We make a tentative source  
560 model 40 km in length with the NEIC main shock location  
561 at the centroid.

#### 562 A1.2. Earthquake B: 8 November 1980, $M_w = 7.3$ , 563 off Trinidad, California

564 [45] Our model for this earthquake is based primarily on  
565 the aftershock pattern shown in the plot of 1980–1986  
566 northern California seismicity of Eaton [1987] and Hill *et al.*  
567 [1990], with relocations by J.P. Eaton using phase data from  
568 the TERA Corporation and NCSN (Figure 2, earthquakes A  
569 and B). The aftershock distribution contains four distinct  
570 clusters, hereafter referred to by the numbering system used  
571 in Figures 2 (earthquake A) and 4. Clusters 1 and 2 define a  
572 N50°E trend consistent with the Global CMT focal mech-  
573 anism and are inferred to be on the rupture. Cluster 1, which  
574 trends northeast from 41°N, 124.9°W and includes the main  
575 shock hypocenter, is east of the surface trace of the Cascadia  
576 subduction zone, indicating that the northeastern section of  
577 the rupture occurred in the subducting Gorda slab. Cluster 2  
578 is southwest of cluster 1 and continues the N50°E trend;  
579 however, the *Chaytor et al.* [2004] faults strike ~65° nearby,  
580 suggesting that the southwest section of the rupture may  
581 have bent toward a more easterly strike. Clusters 3 and 4,  
582 inferred to be off the rupture because of their orientations  
583 and locations, are described in section 6. Assuming a  
584 bilateral rupture after Lay *et al.* [1982], we choose a 100 km  
585 long source model extending 77 km southwest and 23 km  
586 northeast from the NCSN epicenter. The model strikes 51°  
587 in the northeastern 70 km and plunges under the Cascadia  
588 subduction zone in the northeasternmost 50 km. The  
589 megathrust is assumed to strike 350° and dip 9°, so a ver-  
590 tical fault striking 51° within the downgoing slab would  
591 plunge 7.5° along strike; the model simulates this plunge by  
592 “stepping down” 1 km for every 7.7 km along strike. The  
593 model strikes 65° in the southwest 30 km, following  
594 *Chaytor et al.* [2004] faults.

#### 595 A1.3. Earthquake C: 24 August 1983, $M_w = 6.1$ , 596 off Petrolia, California

597 [46] The main NCSN aftershock cluster is 10–25 km  
598 offshore at 20–30 km depth, but the NCSN main shock  
599 location lies 50 km offshore at 12 km depth (Figure 2,  
600 earthquake C). The NEIC main shock location, which uses  
601 data from 217 stations to the NCSN location’s 42, is 30 km  
602 offshore at 30 km depth. Our model extends updip and  
603 eastward from the NEIC hypocenter, consistent with NCSN

aftershocks. Because of potential errors in NCSN aftershock 604  
locations, stress interactions using this model are poorly 605  
constrained. 606

#### A1.4. Earthquake D: 10 September 1984, $M_w = 6.6$ , 607 Mendocino Fault Zone 608

[47] The NEIC epicenter is on the Mendocino Fault Zone, 609  
consistent with the Global CMT focal mechanism, but NEIC 610  
aftershock locations are 10–20 km south of the fault zone, so 611  
we do not make a source model for this earthquake (Figure 2, 612  
earthquake D). 613

#### A1.5. Earthquake E: 31 July 1987, $M_w = 6.0$ , 614 off Petrolia, California 615

[48] The NCSN hypocenter is on the northeast part of 616  
the aftershock pattern in the northern California double- 617  
difference catalog [Waldhauser and Schaff, 2008] (Figure 2, 618  
earthquake E). The source model which best fits the after- 619  
shock pattern has the hypocenter located 80% of the way to 620  
the northeast corner of the rupture and 80% of the way to the 621  
top of the rupture. 622

#### A1.6. Earthquake F: 13 July 1991, $M_w = 6.8$ , 623 off Brookings, Oregon 624

[49] The northeasternmost NEIC aftershocks suggest a 625  
strike of 225°, consistent with the Global CMT focal 626  
mechanism, but aftershocks southwest of the epicenter trend 627  
195°; local *Chaytor et al.* [2004] faults feature both orienta- 628  
tions (Figure 2, earthquake F). We make two alternate source 629  
models: (1) a 40 km long straight rupture striking 225° with 630  
the NEIC epicenter at the centroid and (2) a 55 km long 631  
rupture whose strike changes from 225° to 195° 12 km 632  
southwest of the epicenter. 633

#### A1.7. Earthquake G: 16 August 1991, $M_w = 6.3$ , 634 off Crescent City, California 635

[50] The NEIC main shock location is more reliable than 636  
the NCSN location at this distance (>100 km) offshore, but 637  
NEIC aftershock locations are inconsistent with the NEIC 638  
epicenter, so we do not make a source model for this 639  
earthquake (Figure 2, earthquake G). 640

#### A1.8. Earthquake H: 17 August 1991 (1929 UTC), 641 $M_w = 6.1$ , Honeydew, California 642

[51] The aftershock pattern in the double-difference cata- 643  
log [Waldhauser and Schaff, 2008] trends northwest and dips 644  
northeast, consistent with the Global CMT focal mechanism 645  
(nodal plane 1) (Figure 2, earthquake H). *McPherson and* 646  
*Dengler* [1992] suggest a southwest or west dipping rup- 647  
ture plane based on local fault orientations and observed 648  
effects at the surface. This orientation is compatible with the 649  
second nodal plane in the Global CMT focal mechanism, but 650  
it is not consistent with the aftershock pattern, and so we 651  
choose a northeast dipping model that uses the double- 652  
difference main shock location as the lower eastern corner of 653  
the rupture plane. Aftershock locations suggest that the 654  
rupture propagated updip and west, a similar rupture direc- 655  
tion to the 1992 Cape Mendocino earthquake [Oppenheimer 656  
*et al.*, 1993]. 657

- 658 **A1.9. Earthquake I: 17 August 1991 (2217 UTC),**  
659  $M_w = 7.1$ , off Crescent City, California
- 660 [52] The NEIC main shock location is more reliable than  
661 the NCSN location at this distance (>100 km) offshore, but  
662 NEIC aftershock locations are inconsistent with the NEIC  
663 epicenter, so we do not make a source model for this  
664 earthquake (Figure 2, earthquake I).
- 665 **A1.10. Earthquake J: 25 April 1992,  $M_w = 6.9$ ,**  
666 **Cape Mendocino, California**
- 667 [53] We use the *Oppenheimer et al.* [1993] slip model and  
668 taper the slip at the edges (Figure 2, earthquake J).
- 669 **A1.11. Earthquake K: 26 April 1992 (0741 UTC),**  
670  $M_w = 6.5$ , off Cape Mendocino, California
- 671 [54] The hypocenter in the northern California double-  
672 difference catalog [*Waldhauser and Schaff*, 2008] is at the  
673 northwestern end of the aftershock distribution (Figure 2,  
674 earthquakes K and L). Based on the double-difference  
675 aftershock pattern, Figure 3b of *Oppenheimer et al.* [1993],  
676 and the apparent stress of 40 bars calculated by *Choy and*  
677 *McGarr* [2002], we choose a rupture 12.5 km long and  
678 6.25 km wide extending southeast from the epicenter. Few  
679 aftershocks were recorded at the depth of this earthquake in  
680 the 3.5 h period between this shock and L, and they do not  
681 define a linear pattern, so this model is poorly constrained.
- 682 **A1.12. Earthquake L: 26 April 1992 (1118 UTC),**  
683  $M_w = 6.6$ , off Cape Mendocino, California
- 684 [55] The apparent stress of 164 bars calculated by *Choy*  
685 *and McGarr* [2002] suggests a small rupture area with a  
686 high average slip (Figure 2, earthquakes K and L). Based on  
687 aftershock locations and Figure 3b of *Oppenheimer et al.*  
688 [1993], we choose a rupture 10 km wide and 5 km long  
689 extending southeast and updip from the NCSN hypocenter.  
690 A rupture plane is not visible in the cluster of aftershocks of  
691 this shock and K, so this model is poorly constrained.
- 692 **A1.13. Earthquake M: 1 September 1994,  $M_w = 7.0$ ,**  
693 **Mendocino Fault Zone**
- 694 [56] The apparent stress of 165 bars calculated by *Choy*  
695 *and McGarr* [2002] suggests a small rupture area with a  
696 high average slip (Figure 2, earthquake M). The NEIC  
697 epicenter is at the center of the NEIC aftershock distribution,  
698 suggesting a bilateral rupture, while *Dengler et al.* [1995]  
699 infer that the rupture propagated unilaterally to the east.  
700 We make a model for each scenario. Each source is 15 km  
701 long and 7.5 km wide, uses the Global CMT focal mecha-  
702 nism and scalar moment, and has a calculated average slip  
703 of 10.7 m.
- 704 **A1.14. Earthquake N: 19 February 1995,  $M_w = 6.6$ ,**  
705 **Southern Gorda Zone**
- 706 [57] NEIC aftershock locations are roughly consistent  
707 with the NEIC main shock location, but they do not define a  
708 linear pattern which would indicate a rupture plane (Figure 2,  
709 earthquakes N and O). We make a tentative source model  
710 which uses the NEIC main shock location as the centroid.
- A1.15. Earthquake O: 16 March 2000,  $M_w = 5.9$ ,**  
**Mendocino Fault Zone**
- [58] NEIC aftershocks are sparse but roughly consistent  
with the NEIC main shock location, so we make a tentative  
source model with the NEIC location at the centroid  
(Figure 2, earthquakes N and O).
- A1.16. Earthquake P: 15 June 2005,  $M_w = 7.2$ ,**  
**off Eureka, California**
- [59] We use the G. Shao and C. Ji (2005) slip model,  
excluding the southwest 12 km, northeast 18 km, and bottom  
15 km of their 102 km  $\times$  35 km model because of the low slip  
values in those sections (Figure 2, earthquakes P, Q, and R).
- A1.17. Earthquake Q: 17 June 2005,  $M_w = 6.6$ ,**  
**Southwest Gorda Zone**
- [60] The Global CMT focal mechanism is consistent with  
the orientation of the *Chaytor et al.* [2004] faults near the  
epicenter, but NEIC aftershock locations are sparse (Figure 2,  
earthquakes P, Q, and R). We make a tentative source model  
with the NEIC location at the centroid.
- A1.18. Earthquake R: 28 November 2008,  $M_w = 5.9$ ,**  
**Mendocino Fault Zone**
- [61] NEIC aftershocks are sparse but roughly consistent  
with the NEIC main shock location, so we make a tentative  
source model with the NEIC location at the centroid  
(Figure 2, earthquakes P, Q, and R).
- A1.19. Earthquake S: 10 January 2010,  $M = 6.5$ ,**  
**off Ferndale, California**
- [62] We use the updated D. Dreger (unpublished  
report, 2010, available at [http://seismo.berkeley.edu/~dreger/jan102010\\_ff\\_summary.pdf](http://seismo.berkeley.edu/~dreger/jan102010_ff_summary.pdf)) finite fault model (Figure 2,  
earthquakes S and T).
- A1.20. Earthquake T: 4 February 2010,  $M_w = 5.9$ ,**  
**off Cape Mendocino, California**
- [63] As this is the most recent  $M \geq 5.9$  earthquake, we do  
not make a source model for this earthquake, but we calcu-  
late stress changes imparted by other earthquakes at its  
epicenter (Figure 2, earthquakes S and T).
- A2. Large Historical Earthquakes**
- [64] Locations and focal mechanisms are too poorly  
constrained to support source models for earthquakes in the  
Gorda zone before 1976, but we consider two very large  
pre-1976 shocks for which slip models have been built  
based on coseismic deformation.
- A2.1. The 26 January 1700,  $M \sim 9$ , Cascadia**  
**Subduction Zone**
- [65] The most detailed model for the 1700 Cascadia  
earthquake [*Pollitz et al.*, 2008] is made up of 115 km long  
rectangular patches with slip vectors calculated from fitting  
of a postseismic viscoelastic model. Stress changes imparted  
by this model are unreliable close to the source because they  
are controlled by the straight edges of the patches. Addi-  
tionally, the margin of uncertainty in the 1700 slip distribu-  
tion exceeds the size of the Gorda deformation zone itself. For  
these reasons, we cannot reliably calculate the stress change  
imparted to Gorda zone faults by the 1700 earthquake.

766 **A2.2. 18 April 1906,  $M = 7.8$ , San Andreas Fault**

767 [66] To calculate the Coulomb stress changes imparted by  
768 the 1906 San Andreas earthquake to the Gorda deformation  
769 zone, we use the *Song et al.* [2008] variable slip model,  
770 which is determined from a joint geodetic and seismic  
771 inversion. The northernmost 40 km of this model deviates by  
772 5–10 km from the San Andreas Fault trace in the USGS  
773 Quaternary Fault and Fold Database (Figure 2, earthquake Z).

774 [67] **Acknowledgments.** We thank David Oppenheimer, Patricia  
775 McCrory, and Ruth Harris for reviews; Volkan Sevilgen and Shinji Toda  
776 for technical assistance; Chris Goldfinger and Jason Chaytor for active fault  
777 data; Felix Waldhauser and David Schaff for the double-difference catalog;  
778 and Robert McPherson, Charles Sammis, and Lori Dengler for input.

779 **References**

780 Cande, S. C., and D. V. Kent (1995), Revised calibration of the geomag-  
781 netic polarity timescale for the Late Cretaceous and Early Cenozoic,  
782 *J. Geophys. Res.*, *100*(B4), 6093–6095, doi:10.1029/94JB03098.  
783 Chan, C. H., and R. S. Stein (2009), Stress evolution following the 1999  
784 Chi-Chi, Taiwan, earthquake: Consequences for afterslip, relaxation,  
785 aftershocks, and departures from Omori decay, *Geophys. J. Int.*, *177*,  
786 179–192, doi:10.1111/j.1365-246X.2008.04069.x.  
787 Chaytor, J. D., C. Goldfinger, R. P. Dziak, and C. G. Fox (2004), Active  
788 deformation of the Gorda plate: Constraining deformation models with  
789 new geophysical data, *Geology*, *32*, 353–356, doi:10.1130/G20178.2.  
790 Choy, G. L., and A. McGarr (2002), Strike-slip earthquakes in the oceanic  
791 lithosphere: Observations of exceptionally high apparent stress, *Geophys.*  
792 *J. Int.*, *150*, 506–523, doi:10.1046/j.1365-246X.2002.01720.x.  
793 Dengler, L., K. Moley, R. McPherson, M. Pasyanos, J. W. Dewey, and  
794 M. Murray (1995), The September 1, 1994 Mendocino Fault earth-  
795 quake, *Calif. Geol.*, *48*, 43–53.  
796 Eaton, J. P. (1987), Dense microearthquake network study of northern  
797 California earthquakes, in *Observatory Seismology*, pp. 200–225, Univ.  
798 of Calif. Press, Berkeley.  
799 Goldfinger, C., et al. (2008), Late Holocene rupture of the San Andreas  
800 Fault and possible stress linkage to the Cascadia Subduction Zone, *Bull.*  
801 *Seismol. Soc. Am.*, *98*, 861–889, doi:10.1785/0120060411.  
802 Harris, R. A., R. W. Simpson, and P. A. Reasenber (1995), Influence of  
803 static stress changes on earthquake locations in southern California,  
804 *Nature*, *375*, 221–224, doi:10.1038/375221a0.  
805 Henstock, T. J., and A. Levander (2003), Structure and seismotectonics of  
806 the Mendocino Triple Junction, California, *J. Geophys. Res.*, *108*(B5),  
807 2260, doi:10.1029/2001JB000902.  
808 Hill, D. P., J. P. Eaton, and L. M. Jones (1990), Seismicity, 1980–1986, in  
809 *The San Andreas Fault System, California*, edited by R. E. Wallace, *U.S.*  
810 *Geol. Surv. Prof. Pap.*, *1515*, 115–151.  
811 Jachens, R., and A. Griscom (1983), Three-dimensional geometry of the  
812 Gorda Plate beneath northern California, *J. Geophys. Res.*, *88*(B11),  
813 9375–9392, doi:10.1029/JB088iB11p09375.

King, G. C. P., R. S. Stein, and J. Lin (1994), Static stress changes and the  
814 triggering of earthquakes, *Bull. Seismol. Soc. Am.*, *84*, 935–953. 815  
Lay, T., J. W. Given, and H. Kanamori (1982), Long-period mechanism of  
816 the November 8, 1980 Eureka, California earthquake, *Bull. Seismol. Soc.*  
817 *Am.*, *72*, 439–456. 818  
McCrory, P. A., J. L. Blair, D. H. Oppenheimer, and S. R. Walter (2004),  
819 Depth to the Juan De Fuca slab beneath the Cascadia Subduction Margin  
820 —A 3-D model for sorting earthquakes, *Data Series DS-91*, version 1.1,  
821 U.S. Geol. Surv., Menlo Park, Calif. 822  
McPherson, R. C., and L. A. Dengler (1992), The Honeydew earthquake,  
823 *Calif. Geol.*, *45*, 31–39. 824  
Oppenheimer, D. H., et al. (1993), The Cape Mendocino, California, earth-  
825 quakes of April 1992: Subduction at the triple junction, *Science*, *261*,  
826 433–438, doi:10.1126/science.261.5120.433. 827  
Pollitz, F. F., P. McCrory, J. Svarc, and J. Murray (2008), Dislocation mod-  
828 els of interseismic deformation in the western United States, *J. Geophys.*  
829 *Res.*, *113*, B04413, doi:10.1029/2007JB005174. 830  
Smith, S. W., R. C. McPherson, M. Niazi, and N. Severy (1982), The  
831 November 1980 Trinidad offshore earthquake and aftershocks, technical  
832 report, Pac. Gas and Electr., San Francisco, Calif. 833  
Smith, S. W., J. S. Knapp, and R. C. McPherson (1993), Seismicity of the  
834 Gorda Plate, structure of the continental margin, and an eastward jump of  
835 the Mendocino Triple Junction, *J. Geophys. Res.*, *98*, 8153–8171,  
836 doi:10.1029/93JB00026. 837  
Song, S. G., G. C. Beroza, and P. Segall (2008), A unified source model for  
838 the 1906 San Francisco earthquake, *Bull. Seismol. Soc. Am.*, *98*, 823–  
839 831, doi:10.1785/0120060402. 840  
Stein, R. S., A. A. Barka, and J. H. Dieterich (1997), Progressive failure on  
841 the North Anatolian fault since 1939 by earthquake stress triggering,  
842 *Geophys. J. Int.*, *128*, 594–604, doi:10.1111/j.1365-246X.1997.tb05321.x. 843  
Thatcher, W., G. Marshall, and M. Lisowski (1997), Resolution of fault slip  
844 along the 470-km-long rupture of the great 1906 San Francisco earthquake  
845 and its implications, *J. Geophys. Res.*, *102*, 5353–5367, doi:10.1029/  
846 96JB03486. 847  
Waldhauser, F., and D. P. Schaff (2008), Large-scale relocation of two  
848 decades of Northern California seismicity using cross-correlation and  
849 double-difference methods, *J. Geophys. Res.*, *113*, B08311, doi:10.1029/  
850 2007JB005479. 851  
Wells, D. J., and K. J. Coppersmith (1994), New empirical relationships  
852 among magnitude, rupture length, rupture width, rupture area, and sur-  
853 face displacement, *Bull. Seismol. Soc. Am.*, *84*, 974–1002. 854  
Wilson, D. S. (1986), A kinematic model for the Gorda Deformation Zone  
855 as a diffuse southern boundary of the Juan de Fuca Plate, *J. Geophys.*  
856 *Res.*, *91*, 10,259–10,269, doi:10.1029/JB091iB10p10259. 857  
Wilson, D. S. (1989), Deformation of the so-called Gorda Plate, *J. Geophys.*  
858 *Res.*, *94*, 3065–3075, doi:10.1029/JB094iB03p03065. 859

J. C. Rollins, Department of Earth Sciences, University of Southern 860  
California, 3651 Trousdale Pkwy., Los Angeles, CA 90089-0740, USA. 861  
(chrisrol@usc.edu) 862  
R. S. Stein, U.S. Geological Survey, 345 Middlefield Rd., MS 977, 863  
Menlo Park, CA 94025, USA. (rstein@usgs.gov) 864